NAVSWC TR 91-324

PSEUDOPOTENTIAL BAND CALCULATIONS ALONG A HIGH-SYMMETRY AXIS: PART I Central Potential and the [111] Direction

BY D. Y. AGASSI and J. B. RESTORFF

RESEARCH AND TECHNOLOGY DEPARTMENT

15 JUNE 1991

NAVAL SURFACE WARFARE CENTER

Dahlgren, Virginia 22448-5000 • Silver Spring, Maryland 20903-5000

NAVSWC TR 91-324

PSEUDOPOTENTIAL BAND CALCULATIONS ALONG A HIGH-SYMMETRY AXIS: PART I
Central Potential and the [111] Direction

BY D. Y. AGASSI and J. B. RESTORFF
RESEARCH AND TECHNOLOGY DEPARTMENT

15 JUNE 1991

NAVAL SURFACE WARFARE CENTER
Dahlgren, Virginia 22448-5000 • Silver Spring, Maryland 20903-5000

FOREWORD

An approach particularly suitable for phenomenological band structure calculations of highly anisotropic structures is developed. The approach is based on a cylindrical multipole expansion along a high-symmetry axis and the associated reduction of the Schrodinger equation into a set of coupled, 1-d wave equations. The convergence properties of the multipole expansion are tested for the low Γ-L bands of PbSe. Good convergence is demonstrated.

The authors would like to recognize Dr. E. Callen for his constructive criticism and interest at the early stages of this work and Dr. George Wright for useful scrutiny and encouragement. Thanks are extended also to Drs. T. K. Chu and J. Cullen for stimulating discussions. This work was sponsored by the Naval Surface Warfare Center Independent Research Fund and the Office of Naval Research.

Approved by:

Carl W Larson

CARL W. LARSON, Head
Physics and Technology Division

Accession For	
NTIS GRA&I	☑
DTIC TAB	☐
Unannounced	☐
Justification	
By	
Distribution/	
Availability Codes	
Dist	Avail and/or Special
A-1	

ABSTRACT

A method for band structure calculations along a high-symmetry axis is introduced in this report. It entails a cylindrical coordinate multipole expansion of the wave function and an exact reduction of the three-dimensional Schrodinger equation into a set of one-dimensional wave equations for the multipoles. Group theoretic considerations and energy arguments imply good convergence, regardless of the unit-cell extension along the high-symmetry direction. Band calculations of a test case, PbSe along the [111] direction, demonstrate the good convergence. This method is expected to be particularly useful for structures highly anisotropic along a high-symmetry axis, e.g., superlattices.

CONTENTS

ILLUSTRATIONS

TABLES

SECTION 1

INTRODUCTION

The band model forms the basis for quantitative understanding of electronic properties of crystalline solids. It grew out of a need to reconcile two opposite characteristics: on the one hand solids, e.g., metals, exhibit independent particles (gas) features such as the resistivity, while on the other hand, the expected strong short-range electron-electron repulsion and electron-ion attraction imply a highly correlated system. This basic issue was resolved by the Landau theory of normal Fermi liquids and the concept of pseudopotentials. Landau theory clarified how a strongly correlated fermion system, e.g., electrons, responds to an external one-body probe as if it is comprised of independent constituents--i.e., the quasiparticles. Provided the probe-generated excitations are near the chemical potential (i.e., the Fermi level) the quasiparticles behave as the "bare" fermions except for an effective mass. The pseudopotential concept, on the other hand, describes the apparent weak interaction between near-E_F electrons--the valence electrons--and the ionic cores.[1,2] Underlying this weak interaction is the "cancellation theorem"[3] which states that, at the ionic-core region, the strong valence and core electrons Coulombic repulsion approximately cancels the strong valence-electrons and atomic ion attraction. The net attraction to the ionic cores is consequently weak. When combined, these two fundamental developments lead to the band structure picture: "Real" valence electrons (up to the mass) move independently of each other in an effective, weak, one body, lattice-periodic potential, i.e., the pseudopotential. This electronic motion is described in terms of the appropriate energy bands. The resulting theory yields quantitative agreement with a large body of data such as the frequency dependent dielectric constant, band gaps, electronic transport, etc.

Practical implementation of this physical picture calls for the construction of the pseudopotential and efficient numerical algorithms to solve the associated Schrodinger equation. A large number of approaches exist[4] ranging from empirical pseudopotentials and a small set of basis states to sophisticated, self-consistent, nonlocal pseudopotentials in ab-initio schemes.[5] This spectrum of methods represents a tradeoff between "simple" phenomenological calculations and realistic complex codes. For materials with a large number of atoms in the unit cell, ab-initio calculations are impractical.

The advent of superlattice fabrication, i.e., the growth of layered structures with alternate constituents, poses new challenges to band structure

calculations. A major difficulty is the colossal size of the unit cell, comprised of all unit cells in a superlattice period. As mentioned above, most band structure codes cannot handle very large unit cells. Several methods have been developed to address this difficulty. A popular phenomenological approach is the envelope-function method, supplemented by a prescription for the boundary conditions across the interface.[6] Another approach is ab-initio calculations in a small supercell.[7] Other methods, such as the complex energy band method,[8] combined features of both types of "limits." In this work we introduce yet another method, specifically tailored for phenomenological calculations of highly anisotropic structures along a symmetry axis. The method is predicated on the usage of an empirical pseudopotential[1] and is limited to bands along a high-symmetry direction.

Our starting point is the observation that for an epitaxial superlattice there is a preferred direction in space, i.e., the growth direction, which is invariably also a high symmetry axis. This feature suggests using cylindrical coordinates where the z-axis coincides with the system's high symmetry axis. This leads to the cylindrical coordinates multipole expansion (Section 2). Explicitly, any lattice-periodic function $f(\vec{r})$, e.g., the pseudopotential or the periodic part of the wave function, can be exactly expanded in terms of cylindrical multipoles $f_\ell(g,z')$:

$$f(\vec{r}) = \sum_{\ell=-\infty}^{\infty} \sum_{g} f_\ell(g,z')\, J_\ell(g\,\rho) e^{i\ell\phi} \qquad (1\text{-}1)$$

where ρ,ϕ,z' are the standard cylindrical coordinates, $J_\ell(x)$ is the Bessel function of integer order ℓ, and g varies over a infinite series of positive numbers determined by the geometry of the reciprocal vector space. As Equation (1-1) shows, the ϕ and ρ (transversal) dependence is carried by standard functions. Consequently, the analysis is focused on solving for the z'-dependent multipoles--the "guts" of $f(\vec{r})$. To keep the analysis simple, spin degrees of freedom are omitted at this stage. A subsequent paper covers the appropriate extension.

The usefulness of expansion Equation (1-1) hinges on its convergence properties, i.e., on how many multipoles are needed to describe relevant bands. The other important issue is the simplicity of the equations governing the multipoles. The arguments below and the detailed discussion in the following sections show that Equation (1-1) has good convergence properties and that the multipoles satisfy a set of one-dimensional wave equations.

The good convergence of expansion Equation (1-1) is a consequence of severe limitations on the range of the ℓ and g labels due to group-theoretical and energy considerations. To demonstrate these, we analyze the case of a rocksalt structure along the [111] direction (superlattice or bulk material). As shown in Section 3, the [111] symmetry axis implies that only <u>two</u> ℓ values need be considered! This renders Equation (1-1), in effect, to an expansion in g. The g label, in turn, controls the number of transversal nodes through the Bessel function oscillations. Specifically, for $\ell>0$, $J_\ell(g\,\rho)$ rises from $J_\ell(0) = 0$ to a maximum at $\rho\sim(\ell + 3/2)/g$ and, henceforth, oscillates with a

period $1/g$.[9] (For $\ell = 0$, the latter oscillations start at $\rho = 0$.) Consequently, for a given energy band, all g values up to a cutoff value g_c contribute. A crude estimate of g_c is obtained as follows. In view of the above, "low" energy bands have the least number of ρ-oscillations in the unit cell. To obtain zero ρ-oscillations within the unit cell, it is necessary that $(\ell_m + 3/2)g_c \approx a_T$, where a_T is a typical transversal extension of the unit cell and ℓ_m is a typical ℓ value. (Since only two ℓ values enter, ℓ_m is well defined.) For the test case of bulk PbSe (Section 5) $\ell_m = 3$, $a_T \approx a/2 = 3\text{Å}$ where a is the lattice constant. This gives $g_c \approx 1.5\ \text{Å}^{-1}$ which is approximately the second g value (Section 3, Table 3-1). Thus, for this example, only about four terms in Equation (1-1) need be considered. The above considerations apply equally to a superlattice in the [111] direction since the transversal projection of the lattice constant is the same for a bulk material and a superlattice. Hence, the good convergence is expected to hold for the latter.

The convergence properties of Equation (1-1) are tested numerically for the above case in the entire [111] segment of the Brillouine zone. The results demonstrate good the convergence, with six multipoles or less (Section 3).

The other result of this work is the derivation of an exact set of wave equations for the wave function multipoles (Section 4). Explicitly

$$\left[-g_0^2 + \frac{2m_0}{\hbar^2}E(\vec{k}) + \frac{d^2}{dz'^2}\right]\Psi_\ell(g_0,z') +$$

$$+ \sum_{g_P,g_F} \sum_{m=-2}^{3} A_{\ell,m}(g_0,g_P,g_F)\left[-\frac{2m_0}{\hbar^2}v_m(g_P,z')\right]\Psi_{\ell-m}(g_F,z') = 0 \qquad (1\text{-}2)$$

where $\Psi_\ell(g,z')$ and $v_m(g_P,z')$ are the wave function (unknown) and pseudopotential (known) multipoles, respectively, and the A-coefficients $A_{\ell,m}(g_0,g_P,g_F)$ are geometrical coefficients which depend on the lattice point group and the symmetry of z′ axis. To our knowledge, the geometrical A-coefficients are new constructs which embody the transversal momenta vector addition geometry. The one-dimensionality of Equation (1-2) is advantageous when dealing with a unit cell which extends considerably in the high-symmetry axis direction. It can be solved using any algorithm for coupled ordinary differential equations.

The cylindrical multipoles method developed here has its advantages and limitations. As pointed out above, its primary advantage is good convergence, particularly for highly anisotropic unit-cells. Thus, for example, the method can handle a large number of atoms in the unit cell. On the down side, our method is not valid throughout the Brillouine zone, hence unsuitable for self-consistent calculations.

The paper is organized as follows: In Section 2 we introduce the multipole expansions for the pseudopotential and the wave function. Section 3

is a discussion of the symmetry constraints on the multipole expansion. In Section 4 we derive the basic set of coupled wave equations. The numerical results for bulk PbSe bands in the Γ-Λ-L direction are given in Section 5. Section 6 is a summary and brief discussion.

SECTION 2

THE CYLINDRICAL MULTIPOLE EXPANSION

As in other versions of the empirical pseudopotential approach, it is necessary to solve the three-dimensional Schrodinger equation with a local periodic potential. Unlike other approaches, however, we introduce a cylindrical coordinate system from the outset by choosing the z-axis along a high-symmetry direction of the crystal. This choice has been advocated in the INTRODUCTION as useful in conjunction with superlattices, surfaces, and for anisotropic materials. In this Section we start to develop the approach. For the sake of specificity, it is hereafter assumed that the high-symmetry axis is the [111] direction and the crystal structure is fcc.

The transformation from the (x,y,z) coordinates to the primed coordinates, where z′ is parallel to [111], is given by

$$\begin{bmatrix} x' \\ y' \\ z' \end{bmatrix} = \begin{bmatrix} \frac{1}{2}\sqrt{\frac{2}{3}} & \frac{1}{2}\sqrt{\frac{2}{3}} & -\sqrt{\frac{2}{3}} \\ -\sqrt{\frac{2}{2}} & \sqrt{\frac{2}{2}} & 0 \\ \frac{1}{\sqrt{3}} & \frac{1}{\sqrt{3}} & \frac{1}{\sqrt{3}} \end{bmatrix} \begin{bmatrix} x \\ y \\ z \end{bmatrix} \tag{2-1a}$$

or

$$(\vec{r}') = \hat{R}\,(\vec{r}) \tag{2-1b}$$

The cylindrical coordinates corresponding to (x′, y′, z′) are conventionally defined by

$$x' = \rho\cos\phi, \quad y' = \rho\sin\phi, \quad z' = z' \tag{2-2}$$

where ϕ is the azimuthal angle. It is this cylindrical coordinates system that is used throughout. By the same token, denoting the reciprocal lattice vectors in the unprimed coordinates by $\vec{G} = (G_x, G_y, G_z)$, the vector's components $\vec{G}' = (G_x, G_y, G_z)$ in the primed coordinates are given by

$$(\vec{G}') = \hat{R}\,(\vec{G}) \tag{2-3}$$

since $\vec{G}$ transforms as a polar vector. The fcc reciprocal lattice vectors are given by[10]

$$\vec{G} = \frac{2\pi}{a}\,(-n_1 + n_2 + n_3,\ n_1 - n_2 + n_3,\ n_1 + n_2 - n_3)$$

$$n_1,\ n_2,\ n_3 = 0,\ \pm 1,\ \pm 2,\ \pm 3\ \ldots \tag{2-4}$$

and a is the lattice constant.

To introduce the multipole expansion of a lattice-periodical function, consider first the empirical pseudo potential $v(\vec{r})$[1,11]

$$v(\vec{r}) = \sum_{\vec{G}}{}' \; v(\vec{G})\, e^{i\vec{G}\cdot\vec{r}} = \sum_{\vec{G}'}{}' \; v'(\vec{G}')\, e^{i\vec{G}'\cdot\vec{r}'} = v'(\vec{r}') \tag{2-5}$$

where $v'(\vec{G}') \equiv v(\vec{G}(\vec{G}'))$ and the summation in Equation (2-5) is over a restricted set of $\vec{G}$ vectors of the form Equation (2-4). The coefficients $v(\vec{G})$ are obtained from fitting selected data. Now the exponential in Equation (2-5) can be transcribed to the chosen cylindrical coordinates Equation (2-2):

$$\vec{G}'\cdot\vec{r}' = \rho\, g_P \cos\,(\phi - \delta(\vec{G}_T')) + G_z' z' \tag{2-6}$$

where the transversal reciprocal vector $\vec{G}_T'$ is $\vec{G}_T' \equiv (G_x', G_y')$ and the azimuthal shift angle $\delta(\vec{G}_T)$ and length g_P are defined by:

$$\cos\,\delta(\vec{G}_T') = \frac{G_x'}{g_P}, \qquad \sin\,\delta(\vec{G}_T') = \frac{G_y'}{g_P}$$

$$g_P = \sqrt{(G_x')^2 + (G_y')^2} \tag{2-7a}$$

For the case $g_P = 0$, only the G_z' component survives and, hence, we adopt the convention:

$$\delta(\vec{G}_T') = 0 \quad \text{for} \quad g_P = 0 \tag{2-7b}$$

The multipole expansion is derived by employing the identity[12]

$$e^{iz\cos\phi} = \sum_{\ell=-\infty}^{\infty} i^{\ell}\, J_{\ell}(z)\, e^{i\ell\phi} \tag{2-8}$$

where $J_\ell(z)$ denotes the Bessel function of order ℓ. Applying Equation (2-8) to the RHS of Equation (2-5) gives

$$v'(\vec{r}') = \sum_{g_P} \sum_{\ell=-\infty}^{\infty} v_\ell(g_P,z')\, J_\ell(g_P\,\rho) e^{i\ell\phi} \tag{2-9a}$$

where

$$v_\ell(g_P,z') = i^\ell \sum_{\vec{G}'} v'(\vec{G}')\, e^{iG_z' z'}\, e^{-i\ell\delta(\vec{G}_T')} \tag{2-9b}$$

$$|\vec{G}_T'| = g_P$$

The summation in Equation (2-9b) is over all $\vec{G}'$ such that the length of $\vec{G}_T'$ has the prescribed value g_P. Also, since $J_\ell(0) = \delta_{\ell,0}$,

$$v_\ell(g_P = 0,z') = \delta_{\ell,0}\, v_0(0,z') \tag{2-9c}$$

Equation (2-9c) is consistent with Equation (2-7b).

A similar analysis can be applied to a band wave function $\Psi_{n\vec{k}}(\vec{r})$:[13]

$$\Psi_{n\vec{k}}(\vec{r}) = e^{i\vec{k}\cdot\vec{r}}\, f_{n\vec{k}}(\vec{r}) \quad , \qquad f_{n\vec{k}}(\vec{r}) = \sum_{\vec{L}} \Psi_{n\vec{k}}(\vec{L}) e^{i\vec{L}\cdot\vec{r}} \quad . \tag{2-10}$$

When transformed to the primed coordinates, the lattice periodic function $f_{n\vec{k}}(\vec{r})$ is expanded as in Equation (2-9), while the exponential factor takes the form $\exp[i\vec{k}\cdot\vec{r}] = \exp[i\vec{k}'\cdot\vec{r}'] = \exp[ik'z']$ for $\vec{k}$ vectors pointing in the direction of the high-symmetry axis. For such $\vec{k}$ vectors--the <u>only $\vec{k}$ vectors considered hereafter</u>--the wave function multipole expansion is

$$\Psi'_{n\vec{k}}(\vec{r}') = \sum_{g_F} \sum_{\ell=-\infty}^{\infty} \Psi_{n\ell}(g_F,k',z')\, J_\ell(g_F\,\rho)\, e^{i\ell\phi} \tag{2-11a}$$

where

$$\Psi_{n\ell}(g_F,k',z') = i^\ell \sum_{\vec{L}'} \Psi'_{n\vec{k}}(\vec{L}')\, e^{i(L_z'+k')z'} e^{-i\ell\delta(\vec{L}_T')} \tag{2-11b}$$

$$|\vec{L}_T'| = g_F$$

and the shift angle is defined as in Equation (2-7)

$$\cos \delta(\vec{L}_T') = \frac{L_x'}{g_F} \quad , \quad \sin \delta(\vec{L}_T') = \frac{L_y'}{g_F}$$

$$g_F = \sqrt{(L_x')^2 + (L_y')^2} \quad . \tag{2-12}$$

As before, in Equation (2-11b) $\Psi'(\vec{L}') = \Psi(\vec{L}(\vec{L}'))$ and when $g_F = 0$ then $\delta(\vec{L}_T') = \ell = 0$. The notation in Equation (2-11a) is simplified hereafter by omitting the k',n labels, i.e., $\Psi_{n\ell}(g_F,k',z') = \Psi_\ell(g_F,z')$.

The attractive feature of a multipole (2-9) and (2-11) is that it lumps the contribution of <u>many</u> plane waves, all of which have the same transversal reciprocal vector projection length. Hence, few multipoles may have the capacity of describing well the wave function. In addition, the unknown $\Psi_\ell(g_F,z')$ depends only on one variable and, hence, are considerably easier to solve.

SECTION 3

SYMMETRY PROPERTIES

The multipole expansions Equations (2-9) and (2-11) are general and exact. The particular structure and symmetry of the crystal determines the values of g, ℓ and the locus of the transversal reciprocal vectors $\vec{G}_T'$. We discuss these matters below for the [111] direction and fcc crystals.

Consider first the allowed g values and the locus of $\vec{G}_T'$. These can be calculated from Equations (2-3) and (2-4), with results summarized in Figure 3-1 and Table 3-1. Figure 3-1 shows that all $\vec{G}_T'$ with a given length g fall into hexagonal stars. These stars come either as singles (Figure 3-1a) or as twins (Figure 3-1b). In the latter case the two hexagons are symmetrically tilted with respect to G_x by an angle $\Phi_0(g)$. Therefore, for all $\vec{G}_T'$ the shift angle $\delta(\vec{G}_T')$ has the form

$$\delta(\vec{G}_T') = \pm \left(\Phi_0(g) + \frac{\pi}{3} j\right), \quad j = -2, -1, \ldots +3 \quad . \tag{3-1}$$

The values of g and $\Phi_0(g)$ for the first few $\vec{G}_T'$ stars are given in Table 3-1. Note that the lowest g values are sparse. This is a desirable feature. Since the transversal undulations of the Bessel function $J_\ell(\rho g)$ have a period $\sim g^{-1}$ Å,[9] it is expected that the lowest bands involve g lower than a threshold. Therefore, a sparse sequence of g's implies that only few g values contribute to the lowest bands.

An important consequence of Equation (3-1) is obtained by combining it with definition Equation (2-11b). This gives

$$\Psi_{\ell\pm6}(g_F,z') = - e^{\mp 6i\Phi_0(g_F)} \Psi_\ell(g_F,z') \quad , \quad \text{when } \sin[6\Phi_0(g_F)] = 0 \tag{3-2a}$$

$$\Psi_{\ell\pm12}(g_F,z') = - \Psi_{\ell\pm6}(g_F,z') \frac{\sin[12\Phi_0(g_F)]}{\sin[6\Phi_0(g_F)]} - \Psi_\ell(g_F,z') \quad , \quad \text{when } \sin[6\Phi_0(g_F)] \neq 0 \tag{3-2b}$$

Equations (3-2) (and others not published here) imply that the number of ℓ-independent multipoles is ≤6. This is the first severe constraint on Equation (2-11) due to symmetry. Note also that the four lowest g values in Table 3-1 pertain to Equation (3-2a).

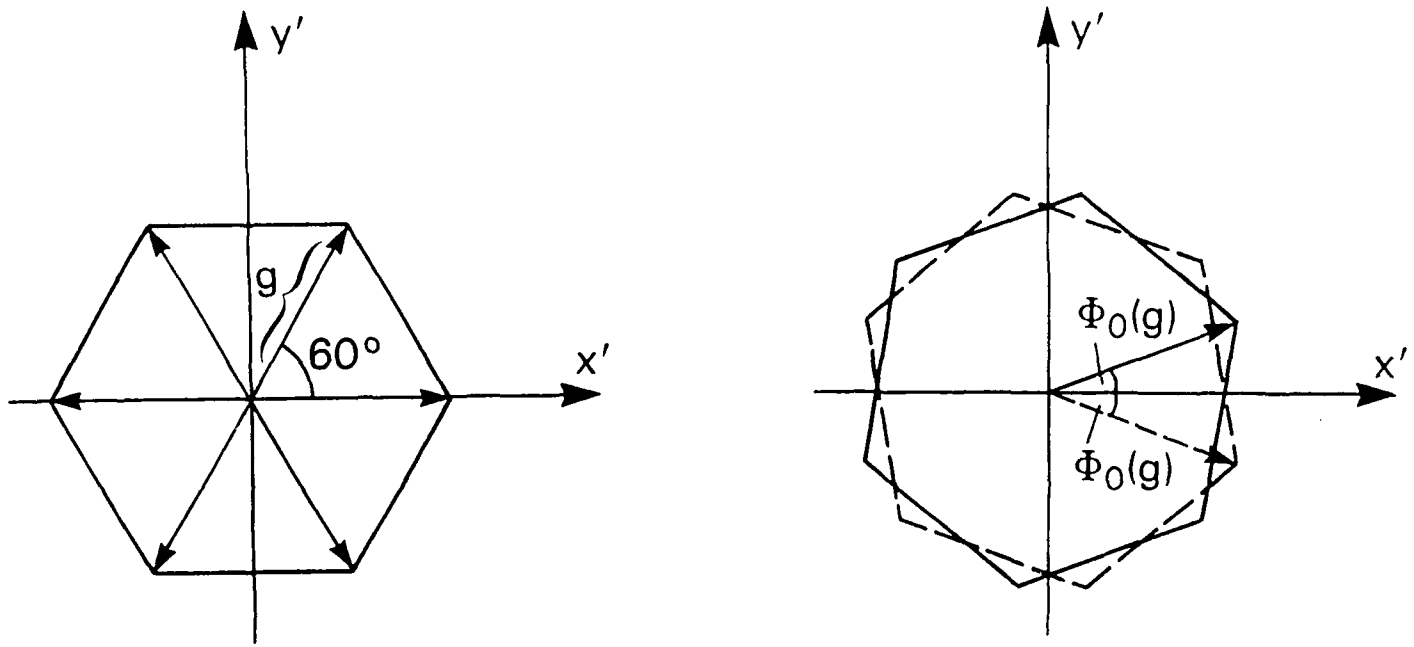

(A)
CASE OF A SINGLE HEXAGON DEFINING THE COORDINATES AND LENGTH G (SEE EQUATION (2-7))

(B)
CASE OF TWO HEXAGONS, SYMMETRICALLY TITLED ABOUT THE $G_{y'}$ AXIS AND THE ANGLE $\Phi_0(g)$ (SEE TABLE 3-1 AND EQUATION (3-1))

FIGURE 3-1. THE LOCUS OF THE fcc RECIPROCAL VECTORS PROJECTIONS UNTO THE PLANE NORMAL TO THE [111] DIRECTION

TABLE 3-1. STRUCTURE OF fcc g-HEXAGONS ASSOCIATED WITH THE [111] DIRECTION

$g = f/a$

	f	g(PbSe)[a] ($Å^{-1}$)	$\Phi_0(g)$ (degrees)	plane wave index N(n)[b]	Hexagon Multiplicity
1.	0.	0.	0.	3j	1
2.	$10.2606 = 2\pi\sqrt{\frac{8}{3}}$	1.6754	0.	≠3j	1
3.	$17.7714 = 2\pi\sqrt{8}$	2.9018	30	3j	2
4.	$20.5207 = 2\pi\sqrt{\frac{32}{3}}$	3.3507	0.	≠3j	1
5.	27.1465	4.4326	19.1066	≠3j	2
6.	30.7813	5.0261	0.	3j	1
7.	35.5430	5.8036	30	3j	2
8.	36.9944	6.0406	13.8979	≠3j	2
9.	41.0414	6.7014	0.	≠3j	1
10.	44.7239	7.3027	36.5868	≠3j	2
11.	47.0193	7.6775	10.8934	3j	2

(a) We used[20] a(PbSe, T = 300K) = 6.1243 Å

(b) Equation (D-8), and j = 0, ± 1, ±2 ...

NOTE: The allowed g values, the hexagon-tilt angle $\Phi_0(g)$ (see Equation 3-1), the L_z' in units of $2\pi/a^*$ and the hexagon multiplicity for a fcc lattice along the [111] direction.

We turn now to the determination of the allowed ℓ values in the wave function multipole expansion, Equation (2-11), and the pseudopotential multipole expansion Equation (2-9). Since the Hamiltonian is invariant under the space group operators, acting on $\Psi_{nk}(\vec{r})$ with any of these operators yields another energy-degenerate wave function associated with another $\vec{k}$ vector. The subgroup of operators which leave a $\vec{k}$ vector unchanged, or yield an equivalent vector $\vec{k} + \vec{L}$ where $\vec{L}$ is a reciprocal lattice vector, is called the "group of wave vector $\vec{k}$".[14] For a given $\vec{k}$, the energy-degenerate wave functions $\Psi^{\alpha}_{nk}(\vec{r})$ ($\alpha = 1,2,\ldots$ is a degeneracy index) span the irreducible representations of the group of the wave vector $\vec{k}$. For symmorphic space groups, the group of wave vector $\vec{k}$ coincide with a subgroup of the associated point group. For non-symmorphic groups (i.e., groups with screw axes and/or glide-reflection planes) the construction of the group of wave vector $\vec{k}$ is more complex, in particular for $\vec{k}$ vectors on the Brillouin zone surface. In the case of PbSe, the space group O_h^5 is symmorphic with the point group O_h.[15]

For the Γ-L direction in the Brillouin zone the relevant groups of wave vector $\vec{k}$ are C_{3v} and D_{3d} for a Λ point and the L point, respectively.[15] These groups and their irreducible representations are discussed in Appendix A. To demonstrate the determination of the allowed ℓ values, consider the two one-dimensional representations at a Λ point,[16] (Table 3-2).

Starting from a general multipole expansion

$$\Psi(\vec{r}') = \sum_{\ell=-\infty}^{\infty} \Psi_{\ell}(\rho,z')e^{i\ell\phi} \tag{3-3}$$

we apply $X_{\pm 1}$ and Y_0, Equation (A-1). These steps give

$$X_{\pm 1}|\Psi(\vec{r}')> = \sum_{\ell=-\infty}^{\infty} \Psi_{\ell}(\rho,z')\ e^{i\ell(\phi \pm \frac{2\pi}{3})}$$

$$= |\Psi(\vec{r}')> = \sum_{\ell=-\infty}^{\infty} \Psi_{\ell}(\rho,z')\ e^{i\ell\phi} \tag{3-4}$$

and

$$Y_0\ |\Psi(\vec{r}')> = \sum_{\ell=-\infty}^{\infty} \Psi_{\ell}(\rho,z')\ e^{-i\ell\phi}$$

$$= \varepsilon|\Psi(\vec{r}')> = \varepsilon \sum_{\ell=-\infty}^{\infty} \Psi_{\ell}(\rho,z')\ e^{i\ell\phi} \tag{3-5a}$$

TABLE 3-2. IRREDUCIBLE REPRESENTATIONS OF C_{3v}[(a)]

REPRESENTATION → OPERATOR	Λ_1	Λ_2	Λ_3
X_0	1	1	$\begin{bmatrix} 1 & 0 \\ 0 & 1 \end{bmatrix}$
$X_{\pm 1}$	1	1	$\begin{bmatrix} \omega^{\pm 1} & 0 \\ 0 & \omega^{\mp 1} \end{bmatrix}$
Y_0 (Plane Reflection)	1	-1	$\begin{bmatrix} 0 & 1 \\ 1 & 0 \end{bmatrix}$
$Y_{\pm 1}$	1	-1	$\begin{bmatrix} 0 & \omega^{\mp 1} \\ \omega^{\pm 1} & 0 \end{bmatrix}$

(a) $\omega = e^{2\pi i/3}$

where

$$\begin{aligned} \varepsilon &= +1 \quad \text{for } \Lambda_1 \ , \\ &= -1 \quad \text{for } \Lambda_2 \ . \end{aligned} \tag{3-5b}$$

Equating both sides of Equation (3-4) yields $e^{\pm i\ell\frac{2\pi}{3}} = 1$ or

$$\ell = 3m \qquad , \qquad m = 0, \pm 1, \pm 2, \ldots \tag{3-6}$$

The same procedure when applied to Equation (3-5) yields the ℓ-parity:

$$\Psi_{-\ell}(\rho,z') = \varepsilon\, \Psi_{\ell}(\rho,z') \tag{3-7}$$

Combining Equations (3-6) and (3-7) gives the multipole expansion of $\Psi_{nk}(\vec{r})$ which transforms as Λ_1, Λ_2 under the C_{3v} operators:

$$\Lambda_1 \colon \Psi(\vec{r}') = |1\rangle = \Psi_0(\rho,z') + 2\Psi_3(\rho,z') \cos 3\phi + 2\Psi_6(\rho,z') \cos 6\phi + \ldots$$

$$\Lambda_2 \colon \Psi(\vec{r}') = |1\rangle = 2i\Psi_3(\rho,z') \sin 3\phi + 2i\Psi_6(\rho,z') \sin 6\phi + \ldots \tag{3-8}$$

The above exercise demonstrates how the symmetry of the group of wave vector $\vec{k}$ severely restricts the multipole expansion ℓ values and determines the ℓ-parity (i.e., a relation between $\Psi_{-\ell}(\rho_F,z')$ and $\Psi_{\ell}(\rho_F,z')$). The treatment of the two dimensional representation Λ_3 is given in Appendix B with the following multipole expansion

$$|1\rangle = \ldots + \Psi_{-2}(\rho,z')e^{-2i\phi} + \Psi_1(\rho,z')e^{i\phi} + \Psi_4(\rho,z')e^{4i\phi} + \ldots$$

Λ_3:

$$|2\rangle = \ldots + \Psi_4(\rho,z')e^{-4i\phi} + \Psi_1(\rho,z')e^{-i\phi} + \Psi_{-2}(\rho,z')e^{+2i\phi} + \ldots \tag{3-9}$$

Note that both in Equations (3-8) and (3-9) the ρ dependence is retained in a multipole $\Psi_{\ell}(\rho,z')$. When the ρ-dependent Bessel function (see Equation (2-11a)) is factored out, the ℓ-parity of $\Psi_{\ell}(g,z')$ are those listed in Table 3-3.

At the L point the group of wave vector $\vec{k}$ is D_{3d}[15] which contains in addition to the C_{3v} operations the z'-inversion (Equation (A-1)). Consequently, the multipoles have in addition a definite z'-parity (i.e., the phase relation between $\Psi_{\ell}(g_F,z')$ and $\Psi_{\ell}(g_F,-z')$). Following the same steps as above yields the sequences of allowed ℓ values for all representations, see Table 3-4.

The pseudopotential, Equation (2-5), is by construction invariant under all space group operations, in particular under the groups of wave vector $\vec{k}$. Therefore, it transforms as the <u>scalar</u> representation under the C_{3v} and D_{3d}

TABLE 3-3. MULTIPOLE CONTENT OF THE C_{3v} IRREDUCIBLE REPRESENTATIONS

IRREDUCIBLE REPRESENTATION	ℓ-values[a]	ℓ-parity π_ℓ[b]	d
Λ_1	$\|1\rangle$: $\ell = 3m$	$(-1)^\ell$	1
Λ_2	$\|1\rangle$: $\ell = 3m$, $m \neq 0$	$-(-1)^\ell$	1
Λ_3	$\|1\rangle$: $\ell = 3m + 1$ $\|2\rangle$: $\ell = 3m - 1$	$-\begin{bmatrix} 0 & (-1)^m \\ (-1)^m & 0 \end{bmatrix}$	2

(a) $m = 0, \pm 1, \pm 2, \ldots$.

(b) $(\Psi_{-\ell}(g,z')) \equiv \pi_\ell(\Psi_\ell(g,z'))$ where $(\Psi_\ell(g,z')) = \Psi_\ell(g,z')$ or $\begin{bmatrix} \Psi_\ell^{(1)}(g,z') \\ \Psi_\ell^{(2)}(g,z') \end{bmatrix}$.

NOTE: The allowed ℓ values and ℓ-parity for the group C_{3v}.

TABLE 3-4. MULTIPOLE CONTENT OF THE D_{3d} IRREDUCIBLE REPRESENTATIONS

IRREDUCIBLE REPRESENTATION	ℓ-values[a]	ℓ-parity π_ℓ[b]	z-parity π_z[c]	d
L_1	$\|1\rangle$: $\ell = 3m$	$(-1)^\ell$	$(-1)^\ell$	1
L_2	$\|1\rangle$: $\ell = 3m$, $m \neq 0$	$-(-1)^\ell$	$(-1)^\ell$	1
L_1'	$\|1\rangle$: $\ell = 3m$, $m \neq 0$	$-(-1)^\ell$	$-(-1)^\ell$	1
L_2'	$\|1\rangle$: $\ell = 3m$	$(-1)^\ell$	$-(-1)^\ell$	1
L_3	$\|1\rangle$: $\ell = 3m + 1$ $\|2\rangle$: $\ell = 3m - 1$	$-\begin{bmatrix} 0 & (-1)^m \\ (-1)^m & 0 \end{bmatrix}$	$-\begin{bmatrix} (-1)^m & 0 \\ 0 & (-1)^m \end{bmatrix}$	2
L_3'	$\|1\rangle$: $\ell = 3m + 1$ $\|2\rangle$: $\ell = 3m - 1$	$-\begin{bmatrix} 0 & (-1)^m \\ (-1)^m & 0 \end{bmatrix}$	$\begin{bmatrix} (-1)^m & 0 \\ 0 & (-1)^m \end{bmatrix}$	2

(a) $m = 0, \pm 1, \pm 2, \ldots$.

(b) $(\Psi_{-\ell}(g,z')) \equiv \pi_\ell(\Psi_\ell(g,z'))$ where $(\Psi_\ell(g,z')) = \Psi_\ell(g,z')$ or $\begin{bmatrix} \Psi_\ell^{(1)}(g,z') \\ \Psi_\ell^{(2)}(g,z') \end{bmatrix}$.

(c) $(\Psi_\ell(g,-z')) \equiv \pi_z(\Psi_\ell(g,z'))$.

NOTE: The allowed ℓ values, ℓ-parity and z-parity for the group D_{3d}.

operators, i.e., as Λ_1 and L_1, respectively. This imposes further restrictions on the relevant ℓ-values, as demonstrated now.

Consider for example the pseudopotential. For our working example it turns out that at most the four lowest g values contribute (Section 5) and only $0 \leq \ell < 6$ need be considered (Equation (3-2a)). On the other hand, the pseudopotential transforms as the L_1 representation, hence, according to Table 3-4 $\ell = 0, \pm 3, \pm 6, \ldots$. Consequently, the independent pseudopotential multipoles have only two ℓ values e.g., $\ell = 0,3$! All the other multipoles are phase-related. The same considerations when applied to the wave-function (Section 5) reduce drastically the number of independent multipoles.

SECTION 4

THE MULTIPOLES' COUPLED WAVE EQUATIONS

Having established the symmetry properties of the multipole expansion, our goal is to transcribe the Schrodinger equation for $\Psi_{n\vec{k}}(\vec{r})$ into equations for the multipoles $\Psi_\ell(g_F,z')$. We sketch here the derivation while most details are given in Appendix C.

The Schrodinger equation for a given pseudopotential $v(\vec{r})$, is

$$\left[\vec{\nabla}^2 + \frac{2m_0}{\hbar^2}\left(E_n(\vec{k}) - v(\vec{r})\right)\right] \Psi_{n\vec{k}}(\vec{r}) = 0 \qquad (4\text{-}1)$$

where m_0 is the effective electron mass (approximated here by the free electron mass), $E_n(\vec{k})$ is the band energy for a given band index n and momentum $\vec{k}$ and $\Psi_{n\vec{k}}(\vec{r})$ is the wave function. Since $\vec{\nabla}^2$ is a scalar under <u>all</u> three dimensional rotations, the Schrodinger Equation (4-1) in the primed coordinates (Equation (2-1)) takes the form:

$$\left[(\vec{\nabla}')^2 + \frac{2m_0}{\hbar^2}\left(E_n(\vec{k}) - v'(\vec{r}')\right)\right] \Psi'_{n\vec{k}}(\vec{r}') = 0 \qquad (4\text{-}2)$$

Equation (4-2) is now transcribed into an equation for the cylindrical coordinates multipoles Equation (2-2). Expressing the laplacian in the cylindrical coordinates and introducing the multipole expansion of the product

$$X(\vec{r}') = v'(\vec{r}')\,\Psi'_{n\vec{k}}(\vec{r}') = \sum_{g_0} \sum_{\ell=-\infty}^{\infty} X_\ell(g_0,z') J_\ell(g_0\rho) e^{i\ell\phi} \qquad (4\text{-}3)$$

we obtain after some projection manipulations

$$\left[-g_0^2 + \frac{2m_0}{\hbar^2} E(\vec{k}) + \frac{d^2}{dz'^2} \right] \Psi_\ell(g_0,z') - \frac{2m_0}{\hbar^2} X_\ell(g_0,z') = 0 \quad . \qquad (4\text{-}4)$$

To render Equation (4-4) useful it is necessary to express $X_\ell(g_0,z')$ in terms of the underlying multipoles $v_\ell(g_P,z')$ and $\Psi_\ell(g_F,z')$. This is achieved by means of a decomposition theorem (Appendix C) which states that:

$$e^{-i\ell\delta(\vec{G}'_T + \vec{L}'_T)} = \sum_{m=-2}^{3} A_{\ell,m}(g_0,g_P,g_F)\, e^{-im\delta(\vec{G}'_T)}\, e^{-i(\ell-m)\delta(\vec{L}'_T)} \tag{4-5}$$

In Equation (4-5) $\vec{G}'_T$ and $\vec{L}'_T$ are two transversal reciprocal vectors of lengths g_P and g_F, respectively, g_0,g_P, and g_F add up to the triangle defined in Figure 4-1 and $A_{\ell,m}(g_0,g_P,g_F)$ are geometrical coefficients given in Table 4-1. In terms of Equation (4-5) it is possible to express $X_\ell(g_0,z')$ Equation (4-3) in a separable form. These steps yield the basic wave equations:

$$\left[-g_0^2 + \frac{2m_0}{\hbar^2} E(\vec{k}) + \frac{d^2}{dz'^2}\right]\Psi_\ell(g_0,z') +$$

$$+ \sum_{g_P,g_F} \sum_{m=-2}^{3} A_{\ell,m}(g_0,g_P,g_F) \left[-\frac{2m_0}{\hbar^2} v_m(g_P,z')\right]\Psi_{\ell-m}(g_F,z') = 0 \tag{4-6}$$

The $\Psi_\ell(g_F,z')$ satisfy the boundary condition implied by the Bloch theorem in the [111] direction, i.e.,

$$\Psi_\ell(g\ ,z' + a^*) = e^{ik'a^*}\, \Psi_\ell(g\ ,z') \tag{4-7a}$$

where k', and a^* are given by

$$k' = K\frac{\pi}{a}\sqrt{3} = K\frac{3\pi}{a^*}, \quad a^* = a\sqrt{3}$$

$$0 < K \leq 1 \tag{4-7b}$$

where the L and a Λ point correspond to $K = 1$ and $K \neq 0$, respectively.

Equations (4-6) and (4-7) are the central results of this work. These equations are exact and valid in the [111] direction. The symmetry of the bands is dictated by the pertaining ℓ-values sequence (Tables 3-3, 3-4). The participating g-values, in ascending order (Table 3-1), are determined by the convergence properties. Equation (4-6) can be interpreted as a set of coupled Kronig Penney models.[17] The coupling reflects the three-dimensional nature of the Schrodinger equation. Note that the diagonal term "$-g_0^2$" represents substraction of the "transversal" kinetic energy from the total energy $E(\vec{k})$ of the band. This is expected since Equation (4-6) involves only z'. The manner in which Equation (4-6) is solved is a matter of convenience. We solved it by transcribing it into a secular equation in a plane wave basis (Appendix D).

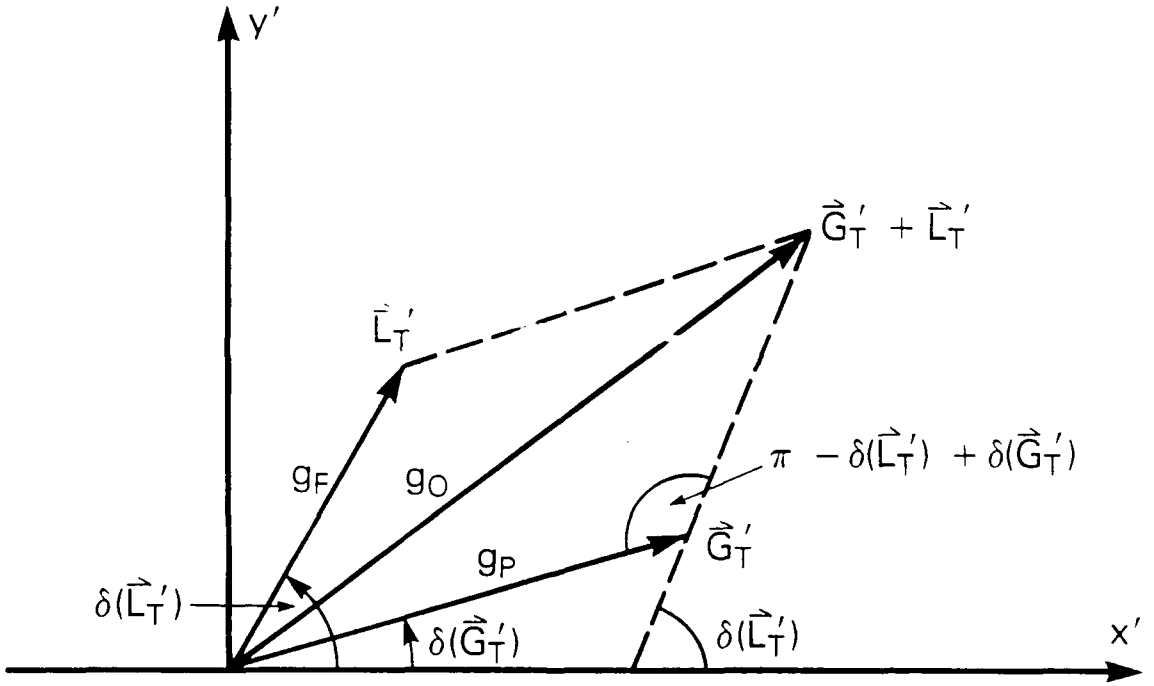

FIGURE 4-1. THE TRANSVERSAL RECIPROCAL VECTORS PARALLELOGRAM DEFINING THE NOTATIONS USED IN SECTION 4

TABLE 4-1. THE A-COEFFICIENTS

g_0	ℓ	m	g_P, g_F	$A_{\ell,m}(g_0, g_P, g_F)$	$\lvert c\rvert$ [a]	TRIANGLE CONFIGURATION
0	0	0	$g_P=g_F=0$	1	∞	●
	0	A.AL. [c]	$g_P=g_F\neq 0$	$\frac{1}{6}(-1)^m$	1	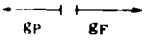
$\neq 0$	A.AL. [c]	0	$g_P=0,\ g_F=g_0$	1	∞	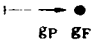
	A.AL. [c]	ℓ	$g_P=g_0,\ g_F=0$	1	∞	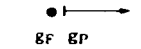
	A.AL. [c]	A.AL. [c]	$g_P\neq 0,\ g_F\neq 0$	$A_{\ell,m}$ [b]	≤ 1	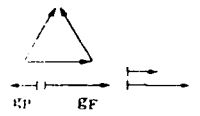

(a) $c = \dfrac{g_0^2 - g_F^2 - g_P^2}{2\, g_F\, g_P}$, $\lvert c\rvert = 0,\ \frac{1}{2},\ \sqrt{\frac{3}{2}},\ 1,\ \infty$ for fcc crystal and the [111] direction.

(b) $A_{\ell,m}(g_0, g_F, g_F) = \frac{1}{3}\, W(\lvert c\rvert)\, \mathrm{Re}\left[B_\ell^{(+)} \exp(im \lvert \arccos(c) \rvert) \right]$

$B_\ell^{(+)} = (((g_F + g_P (c - i\sqrt{1-c^2}))/g_0)^\ell$, $W(\lvert c\rvert) = \frac{1}{2}$ for $\lvert c\rvert = 1$

$= 1$ for $\lvert c\rvert < 1$

(c) A.AL. = Any allowed value.

NOTE: The A-coefficients The triangle configuration corresponds to Figure 4-1. For all cases not quoted in the Table $A_{\ell,m}(g_0, g_P, g_F) = 0$.

SECTION 5

BAND STRUCTURE OF PbSe IN THE Γ-L DIRECTION

In this section we test the multipole expansion convergence, i.e., that a small number of multipoles yields convergent results for $E_n(\vec{k})$. The quotations added to "PbSe" are a reminder that the important spin-orbit interaction is not included at this stage. To keep the discussion focused, the section is subdivided into subsections, each devoted to a specific aspect of the calculation. Further details are given in Appendix D.

THE PSEUDOPOTENTIAL'S MULTIPOLES

The input to the wave equations (Equation (4-6)) are the pseudopotential's multipoles. The empirical pseudopotential for PbSe is comprised of $v(\vec{G})$ such that $|\vec{G}|^2 \leq 12\,(2\pi/a)^2$ [18] (Equation (2-4)) implies that 59 such vectors contribute. When transformed to the primed coordinates the corresponding $\vec{G}_T$ span the first four g-hexagons, i.e., g_P = 0, 1.67, 2.90, 3.35 $Å^{-1}$, Table 3-1. The discussion in Section 3 implies that only ℓ=0,3 need be considered.

The v_0 and v_3 multipoles are depicted in Figures 5-1 and 5-2, respectively. Note that $v_3(g(3),z') = 0$. This is a consequence of the following juxtaposition: Table 3-4 implies in this case that $v_{-3}(g(3),z') = -v_3(g(3),z')$. On the other hand, Equation (3-2a) with $\Phi_0(g(3)) = \pi/6$ (Table 1) gives $v_{-3}(g(3),z') = v_3(g(3),z')$. Hence $v_3(g(3),z') = 0$. Figure 5-3 displays the full pseudopotential along the [111] direction, i.e., (Equation (2-9a)):

$$v'(x' = y' = 0,\ z') = \sum_{g_P} v_0(g_P.z') \qquad (5\text{-}1)$$

The deeper well at $z' = a^*/2$ indicates that it is the anion location since electrons in the lowest bands accumulate there. Correspondingly, the Pb atom is at the origin. This outcome is also inferred from the values of $v(\vec{G})$; see the remark subsequent to Equation (D-6).

The magnitude of the multipoles $v_\ell(g_P,z')$ is indicative of the important g_F values. This is evident from Equation (4-6), where these multipoles provide the coupling between the $\Psi_\ell(g_F,z')$. As Figures 5-1 and 5-2 show, the $g_P = g(2)$ multipole is particularly large. Hence, this g-value is definitely needed. The g = g(1) must be included since it enters when two equal g-values

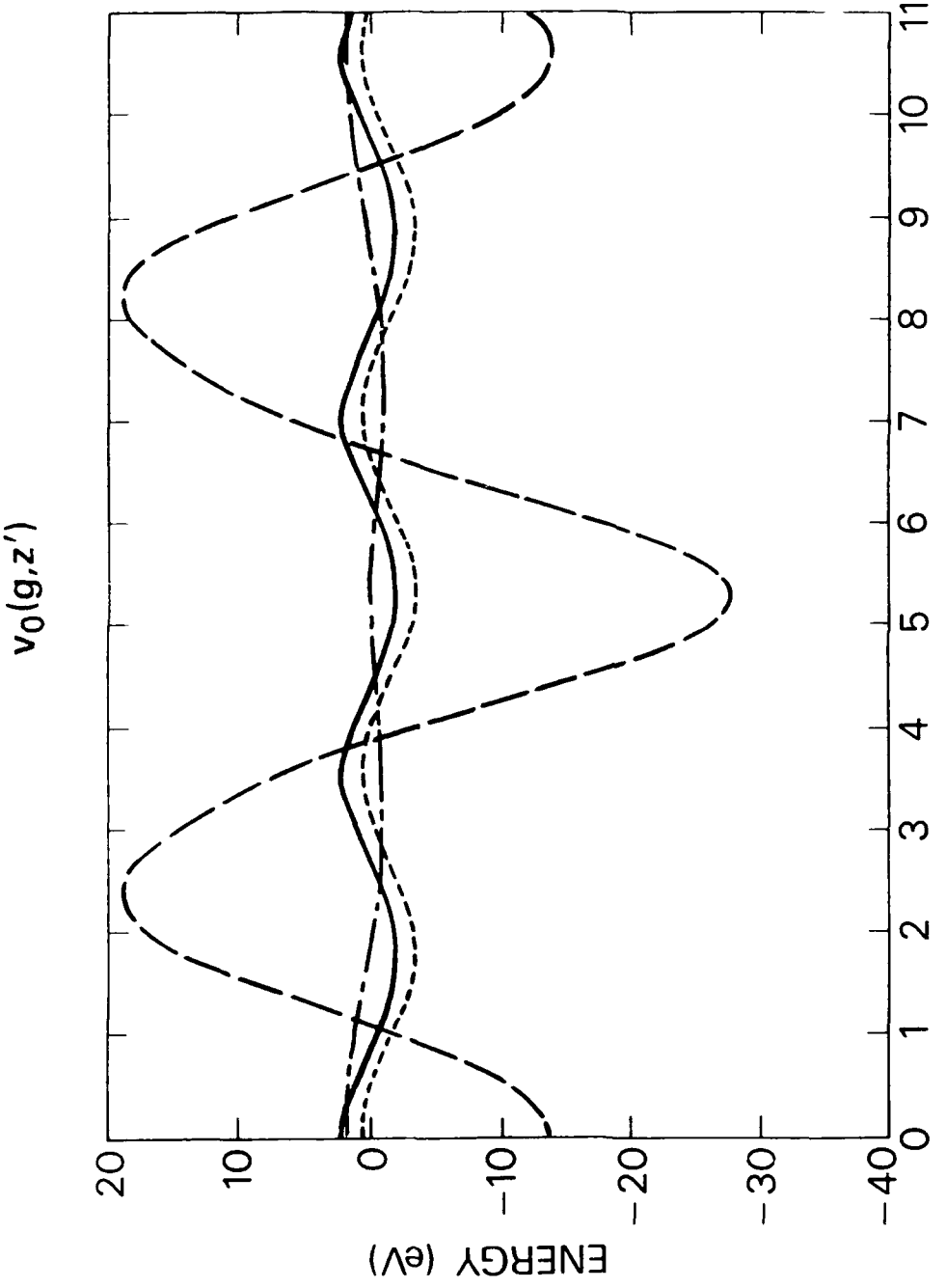

FIGURE 5-1. THE ℓ = 0 MULTIPOLES OF THE PbSe PSEUDOPOTENIAL[18]

Note: The g = g(1), g(2), g(3), and g(4) multipoles are depicted by the solid line (—), long dashed line (— — —), the short dashed line (- -), and dot-dashed line (—·—·), respectively.

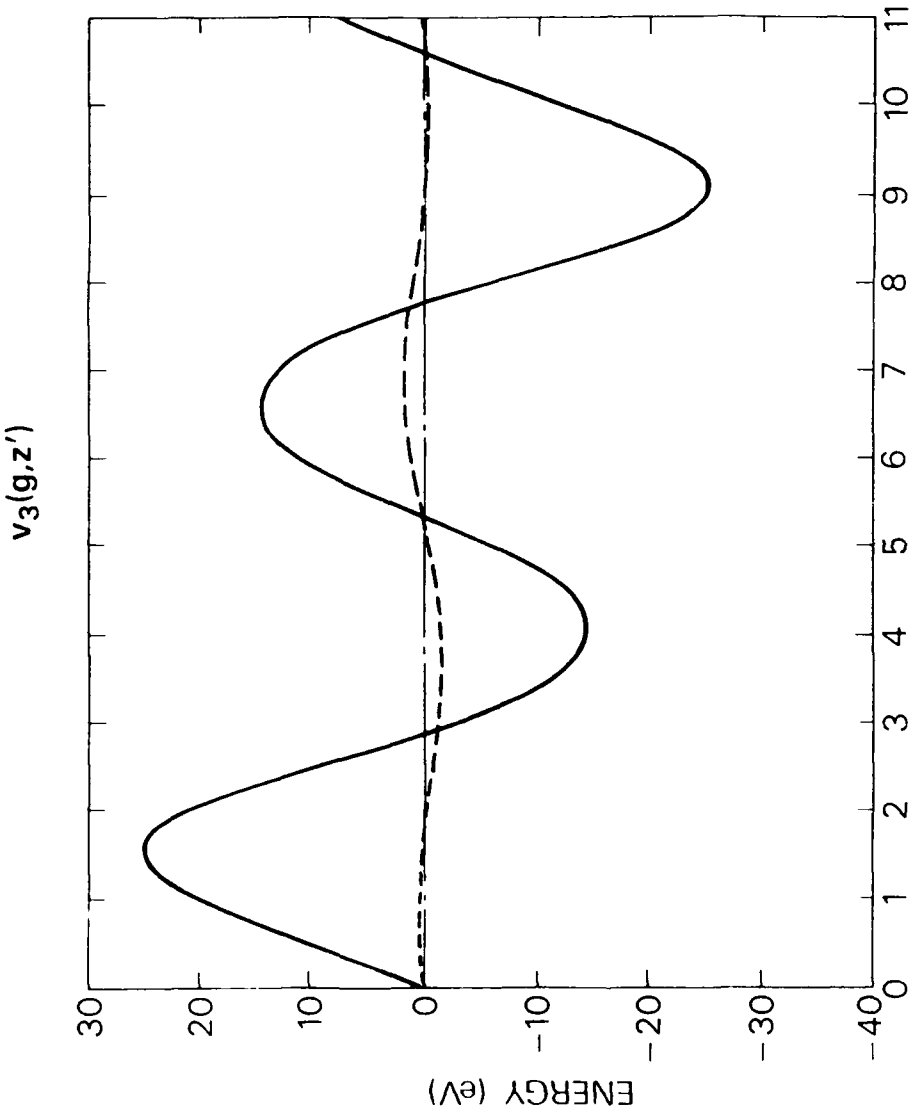

FIGURE 5-2. THE ℓ = 3 MULTIPOLES OF THE PbSe PSEUDOPOTENIAL[18]

Note: The g = g(2), g(3), and g(4) multipoles are depicted by the solid line (—), the dashed-dotted line (—·—·), and the short dashed line (- -), respectively.

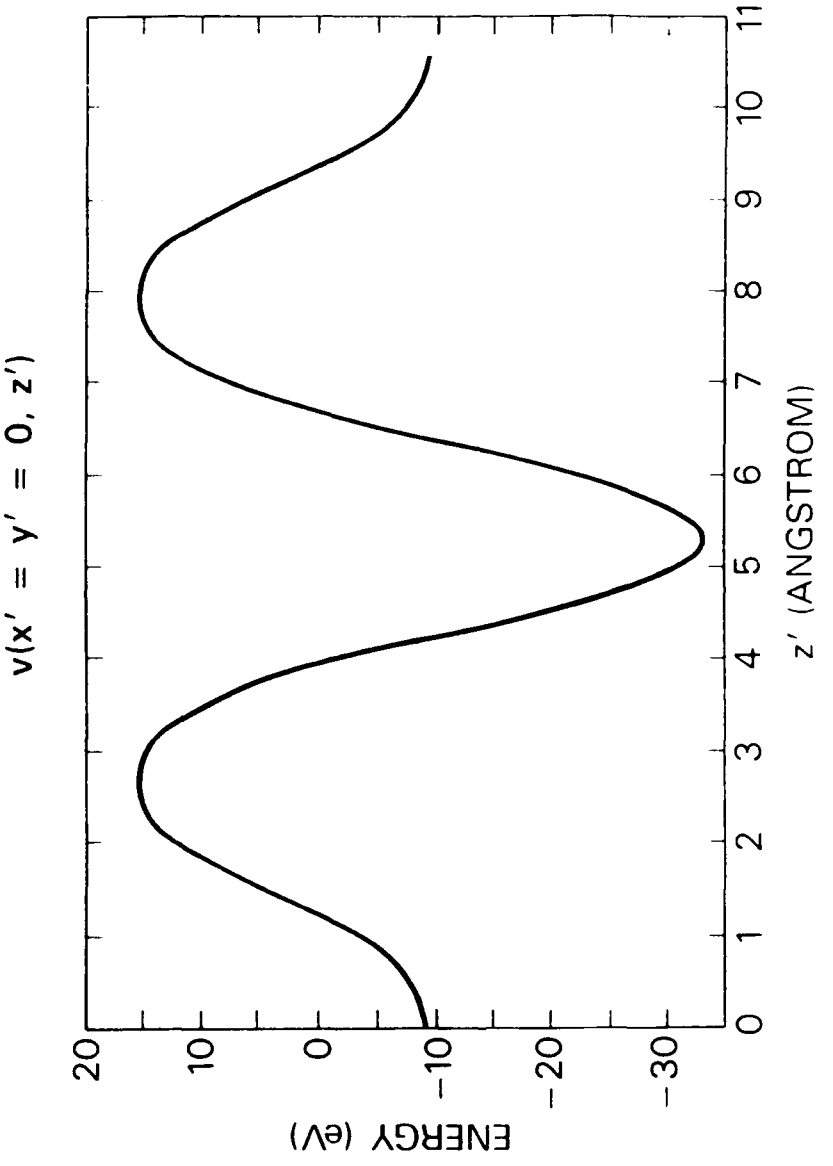

Note: The Pb and Se atoms are at the origin and at z' = a*/2 = 5.304 Å, respectively.

FIGURE 5-3. THE PSEUDOPOTENTIAL ALONG THE z'[111] AXIS (EQUATION (5-1))

multipoles combine. The g = g(3), g(4) are border cases (see Figure 5-1) and their significance can be assessed numerically. All in all, it is necessary to check four g-values, i.e., g(1), g(2), g(3), g(4).

CONVERGENCE

The usefulness of the wave equations (Equation (4-6)) hinges on the convergence properties of the multipole expansion. We examine this issue by calculating the bands along the entire Γ-L direction in the Brillouin zone. The relevant parameter domain is as follows. As argued in subsection Equation (5-1), the potentially important g values are the lowest four (Table 3-1). As Tables 3-3 and 3-4 show (for these g-values), only ℓ = 0,3 need be considered for the L_1, L_2 and Λ_1, representations.[16,19] By the same token, for the L_3, L_3 and Λ_3 representations, only ℓ = -2, +1 need be considered.

In evaluating the calculated bands, we look for a good match with the known band gap at the L-point, the correct number and sequence of the bands (as obtained in other band calculations), and the correct band degeneracies at the Γ-point. The calculations were done considering g-values in ascending order. The calculation of the L_1, L_2 bands and L_3,L_3' bands decouple and, hence, they are considered separately. The results are summarized in Table 5-1 for the L-point and in Figure 5-4 for the entire Γ-L line.

For the L_1, L_2' bands the lowest two g-values at least are needed, i.e., g = g(1),g(2) (Table 3-1). This three-multipole base yields a band gap ΔE=.921 eV, too large in comparison with the experimental value ΔE(PbSe, T = 4.2K) = .165 eV.[20] As Table 5-1 shows, adding the (ℓ=0, g=g(3)) multipole reduces the gap to ΔE=.531 eV, i.e., this multipole is important. On the other hand, the (ℓ=3, g=g(3)) multipole does not change the eigenenergies, i.e., it is decoupled from all other multipoles and, hence, ignored hereafter. Adding the g=g(4) multipole reduces ΔE further by .1 eV. This indicates convergence. The convergent result for the gap, however, is larger than the experimental value. This outcome is expected since the spin orbit interaction, known to reduce the gap, is omitted here.[21] For the (L_3, L_3) representations, a similar pattern emerges (Table 5-1). Including only the g=g(2) multipoles is insufficient. The g=g(3) multipoles give substantial corrections to the pertinent gap, and the g=g(4) multipoles give a relatively smaller correction, indicating convergence. We did not check the effects of modifying m_0, the effective mass. The number and sequence of the calculated bands is the correct one.[15]

The expansion of the above analysis to the entire Γ-L line yields Figure 5-4. Three representative cases are displayed. Figure 5-4a shows the results of a minimum-base. This includes g=g(1),g(2) for the L_1, L_2 representations and g=g(2),g(3) for the (L_3, L_3) representations. The results reproduces the correct trends and the degeneracies at the Γ-point. However, the calculated band gap (ΔE=.921eV, Table 5-1) is much larger than the experimental value. This implies that more multipoles are required to adequately describe the L_1, L_2 representations.

TABLE 5-1. CONVERGENCE OF BAND ENERGIES IN PbSe AT THE L-POINT[a]

		n ⇒	3		4		5		6
ℓ	g								
0	1		*		*		*		*
0	2		*		*		*		*
0	3				*		*		*
0	4								*
3	2		*		*		*		*
3	3						*		
3	4				*		*		*
D_{3d} Representation									
L_2'			10.058		9.432		9.897		9.432
L_1			9.137		8.901		9.013		8.901
L_1			1.496		1.368		1.484		1.368
L_2'			-6.000		-6.919		-6.110		-6.919
$\Delta E^{(b)}$			.921		.531		.884		.531

		n ⇒	2		4		6
ℓ	g						
-2	2		*		*		*
1	2		*		*		*
-2	3				*		*
1	3				*		*
-2	4						*
1	4						*
D_{3d} Representation							
L_3'			11.246		10.712		10.468
L_3			8.593		7.180		6.414
$\Delta E^{(c)}$			2.653		3.532		4.054

(a) Energies are given in eV.

(b) $\Delta E^{(b)} = E(L_2') - E(L_1)$, where the two highest energies in each column are employed.

(c) $\Delta E^{(c)} = E(L_3') - E(L_3)$

(d) n = number of multipoles

NOTE: The six lowest bands of PbSe at the L-point. The upper part of the table lists the total number of multipoles n and the (ℓ,g) pairs considered. The g-values are denoted as the appear in Table 3-1, e.g., g(1) is denoted as 1 in the g-column. An asterisk marks a multipole included in the calculation. The lower part of the table lists the corresponding symmetries, band energies, and the bad gap ΔE_G at the Fermi level.

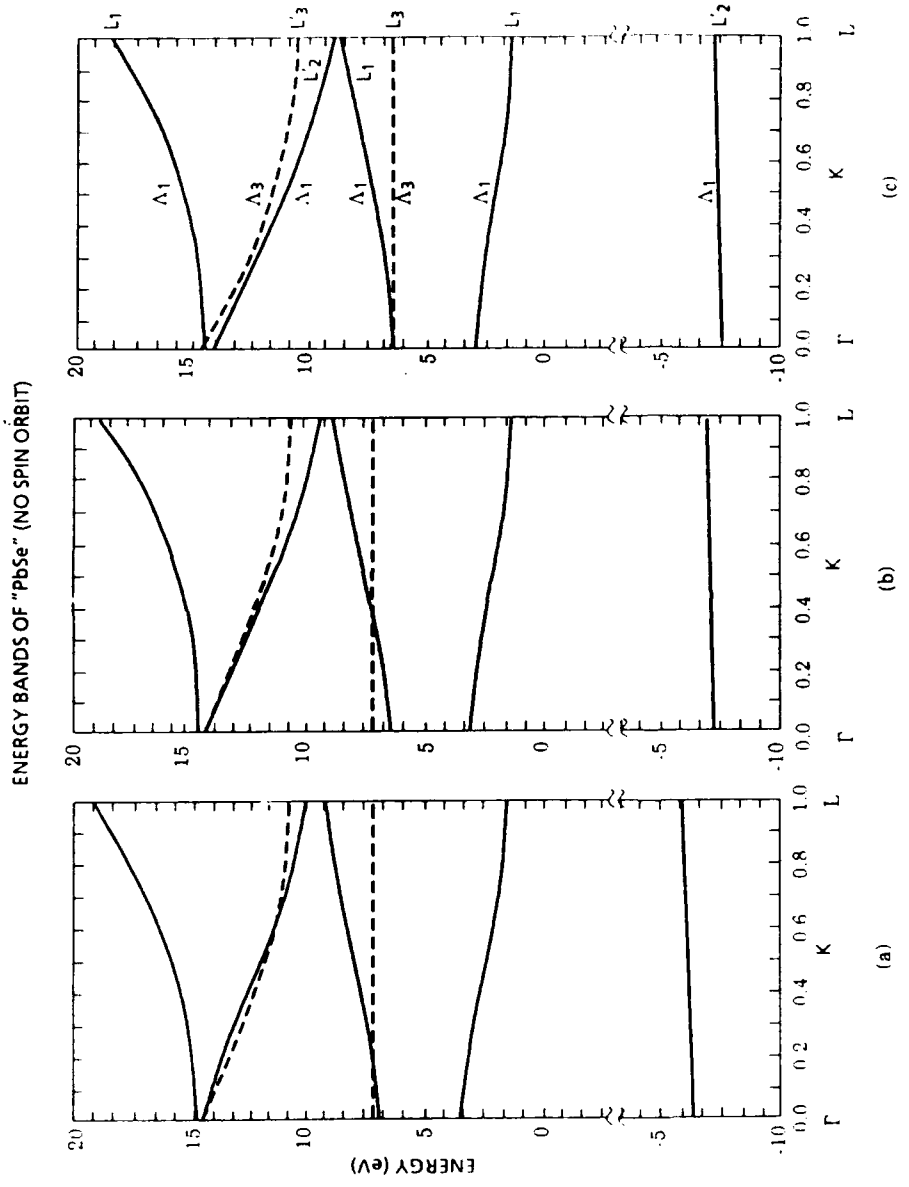

Note: The solid lines show that L1, L2 (Λ_1) bands while the broken lines show the L3, L3 (Λ_3) bands. In Figure 5-4(A), three multipoles were employed for the L1, L2 (Λ_1) bands: $\ell = 0$, g = g(1), $\ell = 0$, g = g(2); $\ell = 3$, g = g(2). For the L3, L3 (Λ_3) bands, four multipoles were employed: $\ell = -1$, g = g(2); $\ell = -1$, g = g(3); $\ell = 2$, g = g(2); $\ell = 2$, g = g(3). In Figure 5-4(B), four multipoles were employed for the L1, L2 (Λ_1) bands: $\ell = 0$, g = g(1); $\ell = 0$, g = g(2); $\ell = 0$, g = g(3); $\ell = 3$, g = g(2). The L3, L3 (Λ_3) bands are as in Figure 5-4(A). In Figure 5-4(C), six multipoles were employed for L1, L2 (Λ_1) bands and for L3, L3 (Λ_3) bands. These multipoles are indicated in Table 5-1 in the n = 6 columns.

FIGURE 5-4. THE CALCULATED PbSe BAND STRUCTURE IN THE Γ-L DIRECTION [18]

In Figure 5-4b we display a "compromise" base; the trends and bands arrangements are as in Figure 5-4. In addition, the calculated L-point band gap is substantially reduced in comparison to Figure 5-4a; however, the Γ-point degeneracies are not reproduced since the L_3, L_3 bands are not evaluated to a similar degree of accuracy. Figure 5-4c shows the convergent calculation with a calculated gap of ΔE=.293eV, (Table 5) and the corect Γ-point degeneracies. Six multipoles are included in this calculation for both L_1, L_2 and L_3, L_3 representations. This result demonstrate that good convergence is achieved for the entire Γ-L line with a small number of multipoles.

SECTION 6

SUMMARY AND DISCUSSION

We developed a method to calculate bands along a high-symmetry axis based on the usage of cylindrical coordinates. This representation leads to the general expansion of a lattice-periodic function in terms of single-variable cylindrical multipoles.

The two central results of this work are (1) the derivation of the wave equations set for the multipoles and (2) the demonstration of good convergence of the multipole expansion in a test case. Using symmetry considerations the three-dimensional Schroedinger equation with a local potential is exactly reduced to a set of coupled ordinary differential equations for the cylindrical multipoles. This reduction employs new A-coefficients which express the constraints of the transversal (two-dimensional) vector addition, in analogy to the Clebsh-Gordan coefficients in the context of three dimensional angular momentum.[23] These coefficients vary with the point group and high symmetry axis. The expressions for the [111] direction in a fcc lattice are derived.

We have also demonstrated good convergence of the cylindrical multipole expansion in a simple case, i.e., PbSe along the [111] direction. These multipoles depend on two discrete indices, denoted by ℓ and g. The former plays the role of projected (longitudinal) angular momentum. The latter is a transversal momentum. Group theoretic considerations limit the number of distinct ℓ-values to two, thus rendering the multipole expansion in effect to an expansion in g. Consequently, the convergence is determined by how many g values contribute. As argued in the INTRODUCTION, the convergence considerations do not depend on the z-extension of the unit cell. Hence, the present approach is expected to be particularly advantageous for highly anisotropic structures, e.g., superlattices. This conclusion can also be stated as follows: Whereas the number of basis functions in a bulk-method grow as N^3, where N is the number of basis functions (e.g., plane waves) needed for each direction in space, the number of basis functions in present method grows as mN, where m is a small number (≤ 6).

The present method bears some similarity to the method of symmetrised plane wave method (SPWM).[24] In both methods the symmetry at the $\vec{k}$-point is utilized to construct "multipoles" to reduce the dimensionality of the secular equation. The present approach has the following new features. It goes one step further by introducing the cylindrical coordinates system. As a result, the present multipoles depend on one coordinate while the SPWM multipoles

depend on three coordinates. Secondly, we derived the set of coupled wave equations, Equation (4-6), for the multipoles. These are exact and do not depend on a specific basis (e.g., plane waves). Future work may employ more efficient algorithms than the one employed in Appendix D. Third, the convergence properties do not depend on the extension of the unit cell in the high-symmetry direction. On the other hand, both SPWM and the present method cannot be readily used for first principle calculations since they do not yield the bands throughout the Brillouin zone. Thus, application of the present method is primarily expected in phenomenological calculations.

The present approach suggests extensions in several directions. The inclusion of the spin orbit interaction is one. Other possibilities are extensions to different high-symmetry axes, the band structure at the Γ point, and different point groups. We hope to address these matters in future publications.

REFERENCES

1. Cohen, M. L., and Heine, V., Solid State Physics, Vol. 24, No. 37, D. Turnbull and F. Seitz, Academic Press, New York, 1970; Cohen, M. L., Physics Today, Jul 1979, p.4C.

2. Bachelet, G. B., Hamann, D. R., and Schlutter, M., Phys. Rev. B, Vol. 26, 1982, p.4199.

3. Philips, J. C., "Bonds and Bands in Semiconductors," Academic Press, New York, NY, 1973. Philips, J. C., and Kleinmann, L., Phys. Rev. Vol. 116, 1959, p.287.

4. Fong, C. Y., "Physics and Chemistry of Materials with Layered Structures," Vol. 3: "Electrons and Phonons in Layered Crystal Structures," Eds., Wieting, T. J., and Schluter, M., D. Reidel Publishing Company, Holland, 1979, p.59-144.

5. The literature is too voluminous to be quoted. For instance, see K. M. Rabe and J. D. Joannopoulos, Phys. Rev. B 32, 2302 1985; R. V. Kasowski, M. H. Tsai, T. N. Rhodin and D. D. Chambliss, Phys. Rev. B 34, 2656 1986; M. Schluter and L. J. Sham, Physics Today, 36, February 1982; J. Callaway and N. H. March, in Solid State Physics, 38, 135, D. Ehernreich, D. Turnball, F. Seitz, Editors (Academic Press, New York, 1984.

6. Bastard, G., Phys. Rev. B Vol. 24, 1981, p.5693; Bastard, G., Phys. Rev. Vol. 25, 1982, p.7584.

7. Van De Walle, C. G. and Martin, R. M., MRS Symposia Proceedings, Vol. 63, Material Research Society, Pittsburg, PA, 1986, p.21.

8. Schulman, J. N. and McGill, T. C. "Synthetic Modulated Structures," Chang, L. L. and Geissen, B. C., Eds., Academic Press, New York, NY, 1985, p.77; Schulman, J. N. and Chang, Y. C., Phys. Rev. Vol. 31, 1985, p.2056; Chang, Y. C., and Schulman, J. N., Phys. Rev. B, Vol. 31, 1985, p.2069.

9. Olver, F. W. J., "Handbook of Mathematical Functions," Abramowitz, M. and Stegun, I. A., Eds., National Bureau of Standards, Applied Mathematics, Vol. 55, 1964, p.355.

REFERENCES (Cont.)

10. Morgan, D. J., "Solid State Theory," Landsberg, P. T., Editor, Wiley-Interscience, London, 1969, p.195 and p.201 ff.

11. Martinez, G., Schluter, M. and Cohen, M. L., Phys. Rev. B, Vol. 11, 1975, p.651.

12. Gradshteyn, I. S., and Ryzhik, I. M., "Table of Integrals Series and Products," Academic Press, New York, NY, 1965, p.973.

13. Ashcroft, N. W., and Mermin, N. D., Solid State Physics, Holt, Rinehart and Winston, New York, NY, 1976, p.133.

14. Morgan, D. J., "Solid State Theory," Landsberg, P. T., Editor, Wiley-Interscience, London, 1969, p.195 and p.201 ff.

15. Dalven, R., Solid State Physics, Vol. 28, Ehrenreich, H., Seitz, F., and Turnbull, D., Eds., Academic Press, New York, NY, 1973, pp.183-184 and p.197.

16. Slater, J. C., "Quantum Theory of Molecules and Solids," Vol. 1, McGraw-Hill, New York, NY, 1965 p.315-318.

17. McKelvey, J. P., "Solid State and Semiconductor Physics," Harper and Row, New York, NY, and John Weatherhill, Inc., Tokyo, JAPAN, 1969, p.212.

18. Kohn, S. E., Yu, P. Y., Petroff, Y., Shen, Y. R., Tsang, Y., and Cohen, M. L., Phys. Rev. B, Vol. 8, 1973, p.1477.

19. Slater, J. C., "Quantum Theory of Molecules and Solids," Vol. 2, McGraw-Hill, New York, NY, 1965, p.380.

20. Nimtz, G., and Schlicht, B., "Narrow Gap Semiconductors" Springer-Verlag, Berlin, 1985, Sec. 3-1.

21. Philips, J. C., "Bonds and Bands in Semiconductors," Academic Press, New York, NY, 1973, p.123.

22. Dalven, R., Solid State Physics, Vol. 28, Ehrenreich, H., Seitz, F., and Turnbull, D., Eds., Academic Press, New York, NY, 1973, pp.183-184 and p.197.

23. Hamermesh, M., "Group Theory" Addison-Wesley, Reading, MA., 1962; Edmonds, A. R., "Angular Momentum in Quantum Mechanics," Princeton University Press, 1957.

24. Schlosser, H., J. Phys. Chem. Solids, Vol. 23, 1962, p.963; Callaway, J., "Quantum Theory of the Solid State," Vol. A, Academic Press, New York, 1974, p.264.

25. Landsberg, P. T., "Solid State Theory," P. T. Landsberg, Editor Wiley-Interscience, London 1969, Ch. B, p.71.

APPENDIX A

IRREDUCIBLE REPRESENTATIONS OF THE D_{3d} and C_{3v} GROUPS

For our purpose it is particularly convenient to use the cylindrical realizations of C_{3v} and D_{3d} groups:[A-1,A-2]

$\underline{C}_{3v}$	$\underline{D}_{3d}$
$X_0\ \Psi(\phi) = \Psi(\phi)$	$X_0\ \Psi(\phi,z) = \Psi(\phi,z)$
$X_{\pm1}\ \Psi(\phi) = \Psi(\phi \pm 2\pi/3)$	$X_{\pm1}\ \Psi(\phi,z) = \Psi(\phi \pm \pi/3, -z)$
$Y_0\ \Psi(\phi) = \Psi(-\phi)$	$X_{\pm2}\ \Psi(\phi,z) = \Psi(\phi \pm 2\pi/3, z)$
$Y_{\pm1}\ \Psi(\phi) = \Psi(-\phi \pm 2\pi/3)$	$X_3\ \Psi(\phi,z) = \Psi(\phi + \pi, -z)$
	$X_0\ \Psi(\phi,z) = \Psi(-\phi, z)$
	$Y_{\pm1}\ \Psi(\phi,z) = \Psi(-\phi \pm \pi/3, -z)$
	$Y_{\pm2}\ \Psi(\phi,z) = \Psi(-\phi \pm 2\pi/3, z)$
	$X_3\ \Psi(\phi,z) = \Psi(-\phi + \pi, -z)$ (A-1)

In Equation (A-1) $\Psi(\phi)$ and $\Psi(\phi, z)$ are arbitrary functions and ϕ is the cylindrical azimuthal angle. Note that Y_0 is a reflection about a plane which includes the z-axis and X_3 is the inversion about the origin.

To derive expeditiously the irreducible representations (Γ), it is necessary to find a convenient basis set U_m. Once such a set is selected, (Γ) is determined according to[A-1]

$$\hat{R}_i\ U_m = \sum_k U_k(\Gamma(\hat{R}_i))_{km} \qquad \text{(A-2)}$$

A-1 Slater, J. C., "Quantum Theory of Molecules and Solids", Vol. 1, McGraw-Hill, New York, NY, 1965 p.315-318.

A-2 Slater, J. C., "Quantum Theory of Molecules and Solids", Vol. 2, McGraw-Hill, New York, NY, 1965, p.380.

where $\hat{R}_i$ is a group operator, Equation (A-1). For the C_{3v} group there are three irreducible representations for which we choose the following bases:

$$\begin{aligned} \Lambda_1: &\quad |1\rangle = e^{3i\phi} + e^{-3i\phi} \\ \Lambda_2: &\quad |1\rangle = e^{3i\phi} - e^{-3i\phi} \\ \Lambda_3: &\quad |1\rangle = e^{i\phi} \\ &\quad |2\rangle = e^{-i\phi} \end{aligned} \quad , \text{ for } C_{3v} \qquad \text{(A-3)}$$

The ensuing irreducible representations are given in Table A-1.

For the D_{3d} group there are six irreducible representations for which the following bases have been chosen:

$$\begin{aligned} L_1': &\quad |1\rangle = (e^{3i\phi} - e^{-3i\phi})\, U(z), \quad U(-z) = U(z) \\ L_2': &\quad |1\rangle = (e^{3i\phi} + e^{-3i\phi})\, U(z), \quad U(-z) = U(z) \\ L_1: &\quad |1\rangle = (e^{3i\phi} + e^{-3i\phi})\, U(z), \quad U(-z) = -U(z) \\ L_2: &\quad |1\rangle = (e^{3i\phi} - e^{-3i\phi})\, U(z), \quad U(-z) = -U(z) \\ L_3': &\quad |1\rangle = e^{i\phi}\, U(z) \\ &\quad |2\rangle = e^{-i\phi}\, U(z) \quad , \quad U(-z) = U(z) \\ L_3: &\quad |1\rangle = e^{i\phi}\, U(z) \\ &\quad |2\rangle = e^{-i\phi}\, U(z) \quad , \quad U(-z) = -U(z) \end{aligned} \quad , \text{ for } D_{3d} \qquad \text{(A-4)}$$

The corresponding irreducible representations are given in Table A-2.

TABLE A-1. IRREDUCIBLE REPRESENTATIONS OF C_{3v}[(a)]

REPRESENTATION → OPERATOR	Λ_1	Λ_2	Λ_3
X_0	1	1	$\begin{bmatrix} 1 & 0 \\ 0 & 1 \end{bmatrix}$
$X_{\pm 1}$	1	1	$\begin{bmatrix} \omega^{\pm 1} & 0 \\ 0 & \omega^{\mp 1} \end{bmatrix}$
Y_0 (Plane Reflection)	1	-1	$\begin{bmatrix} 0 & 1 \\ 1 & 0 \end{bmatrix}$
$Y_{\pm 1}$	1	-1	$\begin{bmatrix} 0 & \omega^{\mp 1} \\ \omega^{\pm 1} & 0 \end{bmatrix}$

(a) $\omega = e^{2\pi i/3}$

TABLE A-2. IRREDUCIBLE REPRESENTATIONS OF D_{3d}[(a)]

REPRESENTATION → OPERATOR	L_1	L_2	L_2'	L_1'	L_3	L_3'
X_0	1	1	1	1	$\begin{bmatrix} 1 & 0 \\ 0 & 1 \end{bmatrix}$	$\begin{bmatrix} 1 & 0 \\ 0 & 1 \end{bmatrix}$
$X_{\pm 1}$	1	1	-1	-1	$\begin{bmatrix} -\Omega^{\pm 1} & 0 \\ 0 & -\Omega^{\mp 1} \end{bmatrix}$	$\begin{bmatrix} \Omega^{\pm 1} & 0 \\ 0 & \Omega^{\mp 1} \end{bmatrix}$
$X_{\pm 2}$	1	1	1	1	$\begin{bmatrix} \Omega^{\pm 2} & 0 \\ 0 & \Omega^{\mp 2} \end{bmatrix}$	$\begin{bmatrix} \Omega^{\pm 2} & 0 \\ 0 & \Omega^{\mp 2} \end{bmatrix}$
X_3 (z parity)	1	1	-1	-1	$\begin{bmatrix} 1 & 0 \\ 0 & 1 \end{bmatrix}$	$\begin{bmatrix} -1 & 0 \\ 0 & -1 \end{bmatrix}$
Y_0 (Plane reflection)	1	-1	1	-1	$\begin{bmatrix} 0 & 1 \\ 1 & 0 \end{bmatrix}$	$\begin{bmatrix} 0 & 1 \\ 1 & 0 \end{bmatrix}$
$Y_{\pm 1}$	1	-1	-1	1	$\begin{bmatrix} 0 & -\Omega^{\mp 1} \\ -\Omega^{\pm 1} & 0 \end{bmatrix}$	$\begin{bmatrix} 0 & \Omega^{\mp 1} \\ \Omega^{\pm 1} & 0 \end{bmatrix}$
$Y_{\pm 2}$	1	-1	1	-1	$\begin{bmatrix} 0 & \Omega^{\mp 2} \\ \Omega^{\pm 2} & 0 \end{bmatrix}$	$\begin{bmatrix} 0 & \Omega^{\mp 2} \\ \Omega^{\pm 2} & 0 \end{bmatrix}$
Y_3	1	-1	-1	1	$\begin{bmatrix} 0 & 1 \\ 1 & 0 \end{bmatrix}$	$\begin{bmatrix} 0 & -1 \\ -1 & 0 \end{bmatrix}$

(a) $\Omega = e^{i\pi/3}$

APPENDIX B

MULTIPOLE CONTENT OF THE IRREDUCIBLE REPRESENTATIONS OF C_{3v} AND D_{3d}

In this appendix we determine the allowed ℓ values pertaining to the irreducible representations of C_{3v} and D_{3d}.

Consider first the two-dimensional representation Λ_3 of C_{3v} (Table A-1). The general multipole expansion of the two basis states is

$$|1\rangle = \sum_{\ell=-\infty}^{\infty} \Psi_\ell^{(1)}(\rho,z')\, e^{i\ell\phi}, \quad |2\rangle = \sum_{\ell=-\infty}^{\infty} \Psi_\ell^{(2)}(\rho,z')\, e^{i\ell\phi} \tag{B-1}$$

We now apply the $X_{\pm1}$ and Y_0 operators (Equation (A-1)) on Equation (B-1) and equate with the irreducible representation in Table A-1. These steps give

$$X_{\pm1}\,|1\rangle = \sum_{\ell=-\infty}^{\infty} \Psi_\ell^{(1)}(\rho,z')\, e^{i\ell(\phi\pm2\pi/3)} = \omega^{\pm1}\,|1\rangle \tag{B-2a}$$

$$X_{\pm1}\,|2\rangle = \sum_{\ell=-\infty}^{\infty} \Psi_\ell^{(2)}(\rho,z')\, e^{i\ell(\phi\pm2\pi/3)} = \omega^{\mp1}\,|2\rangle \tag{B-2b}$$

and

$$Y_0\,|1\rangle = \sum_{\ell=-\infty}^{\infty} \Psi_\ell^{(1)}(\rho,z')\, e^{-i\ell\phi} = |2\rangle \tag{B-3}$$

where $\omega = \exp(2\pi i/3)$. Equating both sides of Equation (B-2) yields

$$\Psi_\ell^{(1)}: \quad e^{\pm i\, 2\pi/3(\ell-1)} = 1 \quad \text{or} \quad \ell = 3m+1$$

$$\Psi_\ell^{(2)}: \quad e^{\pm i\, 2\pi/3(\ell+1)} = 1 \quad \text{or} \quad \ell = 3m-1$$

$$m = 0, \pm1, \pm2, \ldots \tag{B-4}$$

and from Equation (B-3) it follows that

$$\Psi^{(1)}_{-\ell}(\rho,z') = \Psi^{(2)}_{\ell}(\rho,z') \tag{B-5}$$

For the group D_{3d} we use Table A-2 and apply the operators $X_{\pm 1}$, X_3 and Y_0 (Equation (A-1)). This gives for the one dimensional representations

$$X_{\pm 1}\,|1\rangle = \sum_{\ell=-\infty}^{\infty} \Psi_{\ell}(\rho,-z')e^{i\ell(\phi\pm\pi/3)} = \varepsilon\,|1\rangle \tag{B-6}$$

where (Table A-2)

$$\begin{aligned} \varepsilon &= 1 \quad \text{for } L_1,\ L_2 \\ &= -1 \quad \text{for } L_1',\ L_2' \end{aligned} \tag{B-7}$$

In a similar way

$$X_3\,|1\rangle = \sum_{\ell=-\infty}^{\infty} \Psi_{\ell}(\rho,-z')e^{i\ell(\phi+\pi)} = \varepsilon\,|1\rangle \tag{B-8}$$

and

$$Y_0\,|1\rangle = \sum_{\ell=-\infty}^{\infty} \Psi_{\ell}(\rho,z')e^{-i\ell\phi} = \delta\,|1\rangle \tag{B-9}$$

where

$$\begin{aligned} \delta &= 1 \quad \text{for } L_1,\ L_2' \\ &= -1 \quad \text{for } L_1',\ L_2 \end{aligned} \tag{B-10}$$

Equations (B-6) and (B-7) give

$$e^{\pm i\ell\pi/3}\,\Psi_{\ell}(\rho,-z') = e^{\pm i\pi\ell}\,\Psi_{\ell}(\rho,-z') = \varepsilon\,\Psi_{\ell}(\rho,z') \tag{B-11}$$

The LHS of Equation (B-11) holds for $\ell = 3m$, where $m = 0, \pm 1, \pm 2, \ldots$. The RHS of Equation (B-11) gives the z-parity rule, i.e., a relation between $\Psi_{\ell}(\rho,-z')$ and $\Psi_{\ell}(\rho,z')$. Finally, Equation (B-9) yields the ℓ-parity rule

$$\Psi_{-\ell}(\rho,z') = \delta\,\Psi_{\ell}(\rho,z') \tag{B-12}$$

Note that Tables 3-3 and 3-4 of the text refer to $\Psi_{\ell}(g,z')$.

The two-dimensional representations L_3, L_3' are treated as Λ_3 above. Applying $X_{\pm 1}$, X_3 and Y_0 yields equations sufficient to determine the ℓ values and parities.

APPENDIX C

DERIVATION OF EQUATION (4-6) AND THE DECOMPOSITION THEOREM EQUATION (4-5)

To arrive from Equation (4-4) of the main text to the multipoles wave equation Equation (4-6), it is necessary to express $X_\ell(g_0,z')$ in a separable form. The explicit expression of $X_\ell(g_o,z')$ (Equation (4-3)) is:

$$X_\ell(g_0,z') = i^\ell \sum_{\substack{\vec{G}',\vec{L}' \\ |\vec{G}_T'+\vec{L}_T'| = g_0}} v'(\vec{G}')\, \Psi'(\vec{L}')\, e^{i(L_z'+G_z'+k')z'}\, e^{-i\ell\delta(\vec{G}_T'+\vec{L}_T')} \qquad (C\text{-}1)$$

where $\Psi'_{\vec{nk}}(\vec{L}') \equiv \Psi'(\vec{L}')$ and

$$\cos\delta(\vec{G}_T'+\vec{L}_T') = \frac{G_x'+L_x'}{g_0} \quad , \quad \sin\delta(\vec{G}_T'+\vec{L}_T') = \frac{G_y'+L_y'}{g_0}$$

$$g_0 = \sqrt{(G_x'+L_x')^2+(G_y'+L_y')^2} \qquad (C\text{-}2)$$

(for $g_0 = 0$ only $\ell = 0$ is allowed and $\delta(\vec{G}_T'+\vec{L}_T') = 0$). The constraint on the summations in Equation (C-1) reflects the geometry of a triangle formed by vector addition of $\vec{G}_T'$ and $\vec{L}_T'$, see Figure 4-1 in the main text.

The constraint on the summations in Equation (C-1) can be written in a more convenient form as:

$$\sum_{\vec{G}',\vec{L}'} = \sum_{g_P,g_F} \sum_{\vec{G}'} \sum_{\vec{L}'} \qquad (C\text{-}3)$$

$$|\vec{G}_T'+\vec{L}_T'| = g_0 \qquad |\vec{G}_T'| = g_P \qquad |\vec{L}_T'| = g_F$$

$$|\vec{G}_T'+\vec{L}_T'| = g_0$$

In Equation (C-3), the sum over $\vec{L}'$, $\vec{G}'$ is converted to a sum over all possible hexagons of $\vec{G}_T$, $\vec{L}_T$. However, not all hexagons of $\vec{L}_T$ and $\vec{G}_T$ are mutually

compatible: Since $\vec{L}_T'$, $\vec{G}_T'$ and $\vec{L}_T' + \vec{G}_T'$ form a triangle, only those g_P and g_F which form a triangle with the third side of length g_0 are acceptable. The other g_P, g_F combinations are excluded by the constraint $|\vec{L}_T + \vec{G}_T| = g_0$. This constraint is quantified by considering the triangle in Figure 4-1. First we consider non-degenerate triangles (i.e., when g_0, g_P, $g_F \neq 0$ and no angle in the triangle is 0 or π). All other cases are treated thereafter.

The cosine theorem for the triangle in Figure 4-1 gives

$$\cos\left[\delta(\vec{G}_T') - \delta(\vec{L}_T')\right] = \frac{g_0^2 - g_P^2 - g_F^2}{2g_P g_F} = c\,(g_0, g_P, g_F) \equiv c \qquad \text{(C-4)}$$

Hence a triad g_0, g_P, g_F represents a triangle if, and only if, $|c|<1$. The RHS of Equation (C-3) then takes the form

$$\sum_{g_P, g_F} \quad \sum_{\vec{G}'} \quad \sum_{\vec{L}'} \qquad \text{(C-5)}$$

$$|c(g_0, g_P, g_F|<1 \qquad |\vec{G}_T'| = g_P \qquad |\vec{L}_T'| = g_F$$

where $\sum$ in Equation (C-5) indicates a summation only on g_P, g_F such that for a given g_0 the inequality $|c|<1$ holds.

The other source of "coupling" in Equation (C-1) is in the shift phase $\delta(\vec{G}_T' + \vec{L}_T')$. To simplify this term we derive first an identity. Projecting the triangle in Figure 4-1 on the x' and y' axes and adding the two equalities with the imaginary unit factor gives the identity

$$e^{\pm i\delta(\vec{G}_T' + \vec{L}_T')} = \frac{1}{g_0}\left[g_P\, e^{\pm i\delta(\vec{G}_T')} + g_F\, e^{\pm i\delta(\vec{L}_T')}\right] . \qquad \text{(C-6)}$$

On the other hand, inversion of Equation (C-4) gives

$$\delta(G_T') - \delta(\vec{L}_T') = \pm\,\alpha\,, \qquad \alpha = |\arccos(c)| \qquad \text{(C-7)}$$

where the two signs in Equation (4-12) correspond to the two possible triangles (interchanging $\vec{G}_T$ and $\vec{L}_T$) with the same $\vec{G}_T + \vec{L}_T$. Combining Equation (C-4) and (C-6) with the minus sign gives the identity:

$$e^{-i[\delta(\vec{G}_T' + \vec{L}_T') - \delta(\vec{L}_T')]}$$

$$= B_1^{(+)}{}_{\delta(\vec{G}_T') - \delta(\vec{L}_T') - \alpha, 0} + B_1^{(-)}{}_{\delta(\vec{G}_T') - \delta(\vec{L}_T') + \alpha, 0} \qquad \text{(C-8)}$$

where

$$B_1^{(+)} = \frac{1}{g_0}\left[g_F + g_P\left(c - i\sqrt{1-c^2}\right)\right], \quad B_1^{(-)} = (B_1^{(+)})^* \tag{C-9}$$

The Kronecker δ are inserted in Equation (C-8) since the LHS is under the summation in Equation (C-1) and the shift angles $\delta(\vec{G}_T)$, $\delta(\vec{L}_T)$ are discrete. Furthermore, since $\alpha \neq 0$ for a non-degenerate triangle it follows that only one term in Equation (C-8) contributes for given $\delta(\vec{G}_T + \vec{L}_T)$, $\delta(\vec{L}_T)$. Consequently raising both sides of Equation (C-8) to the ℓ-th power one obtains the key result:

$$e^{-i\ell[\delta(\vec{G}_T' + \vec{L}_T') - \delta(\vec{L}_T')]}$$

$$= B_\ell^{(+)}\delta_{\delta(\vec{G}_T') - \delta(\vec{L}_T') - \alpha,0} + B_\ell^{(-)}\delta_{\delta(\vec{G}_T') - \delta(\vec{L}_T') + \alpha,0} \tag{C-10}$$

where

$$B_\ell^{(+)} = (B_1^{(+)})^\ell \quad , \quad B_\ell^{(-)} = (B_\ell^{(+)})^* \tag{C-11}$$

To express the Kronecker δ factors in Equation (C-10) in a separable form, consider their arguments. Since the shift angles $\delta(\vec{G}_T)$, $\delta(\vec{L}_T)$ obey Equation (3-1) we have

$$\delta(\vec{G}_T') - \delta(\vec{L}_T') \pm \alpha = \pi/3\,(j-n) + \Phi_0(g_P) - \Phi_0(g_F) \pm \alpha$$

$$= \pi/3\,(j-n) + \Delta^{\pm} \tag{C-12}$$

Now Equation (C-10) is under the $\vec{G}_T'$, $\vec{L}_T'$ summations of Equation (C-5). This guarantee that at least one triangle $\vec{G}_T$, $\vec{L}_T$ and $\vec{G}_T + \vec{L}_T$, is formed with $|\vec{G}_T + \vec{L}_T| = g_0$. Therefore, as function of j and n, the RHS of Equation (C-12) will vanish for certain j and n. Hence $\Delta^{\pm}$ must equal a multiple of $\pi/3$ and the LHS of Equation Equation (D-12) is always a multiple of $\pi/3$. Obviously this multiple is ≤ 6. Therefore the Kronecker δ in (C-10) can be expressed using the identity[25]

$$\delta_{\frac{\pi}{3}s,0} = \frac{1}{6}\sum_{m=-2}^{3} e^{-i\frac{\pi}{3}ms} \quad , \quad |s| \leq 6 \tag{C-13}$$

Replacing $\pi/3$ s in Equation (C-13) by the LHS of Equation (C-12), the Kronecker δ factors in Equation (C-10) attain a separable form and the decomposition theorem Equation (4-5) follows. Expressing Equation (C-10) in this form and inserting into Equation (C-1) and (C-5) yields the wave equation Equation (4-6).

A similar treatment applies for the degenerate-triangle cases (Figure 4-1). When $g_0 = 0$, only $\ell = 0$ is allowed and $\delta(\vec{G}'_T + \vec{L}'_T) = 0$ in Equation (C-1). Furthermore, since $|\vec{G}'_T + \vec{L}'_T| = 0$, it follows that $|\vec{G}'_T| = |\vec{L}'_T| = g$ and the vectors $\vec{G}'_T$, $\vec{L}'_T$ point back to back. Therefore, Equation (C-1) takes the simple form:

$$X_0(g_0 = 0, z') = \sum_{G'_z,\, L'_z} v'(\vec{G}')\, \Psi'(\vec{L}')\, e^{i(G'_z + L'_z + k')z'}$$

$$+ \sum_{g \neq 0} \sum_{\substack{\vec{G}' \\ |\vec{G}'_T| = g}} \sum_{\substack{\vec{L}' \\ |\vec{L}'_T| = g}} v'(\vec{G}')\, \Psi'(\vec{L}')\, e^{i(G'_z + L'_z + k')z'} \quad * \quad [\delta_{\delta(\vec{G}'_T)-\delta(\vec{L}'_T)-\pi,0} + \delta_{\delta(\vec{G}'_T)-\delta(\vec{L}'_T)+\pi,0}] \qquad \text{(C-14)}$$

The first term in Equation (C-14) corresponds to a triangle degenerated into a point, i.e., $\vec{G}'_T = \vec{L}'_T = 0 = g$. The subsequent lines corresponds to a triangle collapsed into a segment. As can be checked by counting, it is necessary to include the two Kronecker δ terms. However, both Kronecker δ factors are represented in this case by the <u>same</u> expansion Equation (C-13). This is the origin of the "1/6" in Table 4-1 of the main text.

The cases $g_P=0$, $g_F=g_0$ and $g_P=g_0$, $g_F=0$ are trivial: Obviously in these cases $\delta(\vec{G}'_T + \vec{L}'_T) = \delta(\vec{L}'_T)$ and $\delta(\vec{G}'_T)$, respectively and Equation (C-1) is already in a separable form. For the other case with $c = -1$, two Kronecker δ factors contribute in Equation (C-10); however, again both are represented by the same separable expansion Equation (C-13). For the case with $c = 1$, $\vec{G}'_T$ and $\vec{L}'_T$ are collinear and point at the same direction. Hence, Equation (C-10) involves only one Kronecker δ, which leads to the $W(|c|) = 1/2$ factor in Table 4-1

APPENDIX D

NUMERICAL SOLUTION OF THE WAVE EQUATIONS (4-6)

THE PSEUDOPOTENTIAL $v(\vec{r})$

For a crystal with n_A atoms per unit cell, each of specie α, the lattice-periodic pseudopotential is given by

$$v(\vec{r}) = \sum_{\alpha=1}^{n_A} v_\alpha(\vec{r}-\vec{\tau}_\alpha) \tag{D-1}$$

where $\vec{\tau}_\alpha$ is the location of atom α with respect to a chosen origin in the unit cell and $v_\alpha(\vec{r})$ is the "elemental" pseudopotential. Since Equation (D-1) is lattice-periodic, it has the (truncated) fourier expansion

$$v(\vec{r}) = \sum_{\vec{G}}{}' \, e^{i\vec{G}\cdot\vec{r}} \sum_{\alpha=1}^{n_A} S_\alpha(\vec{G}) v_\alpha(\vec{G}) \tag{D-2}$$

where the structure factors $S_\alpha(\vec{G})$ and the "elemental" parameters $v_\alpha(\vec{G})$ are defined by:[4]

$$S_\alpha(\vec{G}) = \frac{1}{n_A} e^{-i\vec{G}\cdot\vec{\tau}_\alpha}, \qquad v_\alpha(\vec{G}) = \frac{n_A}{\Omega} \int_\Omega d\vec{r} \, e^{-i\vec{G}\cdot\vec{r}} \, v_\alpha(\vec{r}) \tag{D-3}$$

In Equation (D-2) $\vec{G}$ has a length smaller that a given cutoff, and in Equation (D-3) Ω is the compound's unit cell volume. The origin of the n_A normalization factor in Equation (D-3) is evident by considering the $n_A = 2$ case: For the elemental $v_\alpha(\vec{G})$, the corresponding volume factor in Equation (D-3) is that of the elemental solid. However, for two atoms per unit cell, Ω is about twice the volume of the elemental unit cell. Therefore, to associate $v_\alpha(\vec{G})$ with the elemental parameters it is necessary to introduce the n_A factors as in Equation (D-3).

For the special case of $n_A = 2$, Equation (D-2) is rewritten in the form

$$\sum_{\alpha=1}^{2} S_\alpha(\vec{G}) v_\alpha(\vec{G}) = S_S(\vec{G}) v_S(\vec{G}) + S_A(\vec{G}) v_A(\vec{G}) \tag{D-4}$$

where

$$v_S(\vec{G}) = \frac{1}{2}\,[v_1(\vec{G}) + v_2(\vec{G})]\ ,\ v_A(\vec{G}) = \frac{1}{2}\,[v_1(\vec{G}) - v_2(\vec{G})]$$

$$S_S(\vec{G}) = S_1(\vec{G}) + S_2(\vec{G})\ \ ,\ S_A(\vec{G}) = S_1(\vec{G}) - S_2(\vec{G}) \qquad \text{(D-5)}$$

For the rocksalt structure with two atoms per unit cell $\vec{\tau}_1 = (0,0,0)$, $\vec{\tau}_2 = a(1/2,1/2,1/2)$, and $\vec{G}$ is given in Equation (2-4). Consequently the structure functions Equation (D-5) take the very simple form:[D-1]

$$S_S(\vec{G}) = \frac{1}{2}\,(1 + \exp[-i\pi(n_1 + n_2 + n_3)]$$

$$S_A(\vec{G}) = \frac{1}{2}\,(1 - \exp[-i\pi(n_1 + n_2 + n_3)] \qquad \text{(D-6)}$$

The values $v_A(\vec{G})$, $v_S(\vec{G})$ for the corresponding non vanishing structure functions Equation (D-6) are fitted.[D-2] These are the values used hereafter. By comparing the quoted values of v_S, v_A with the "elemental" values v_α for Pb and Se[D-2] we conclude that Pb is at the origin and Se is at the midpoint of the [111] diagonal (see also Section 3 and Figure 5-1 of the main text).

NUMERICAL DETAILS

A convenient method for solving the wave equations, Equation (4-6), for the eigenvalues and eigenfunctions is transforming them to a secular equation in a plane wave representation. Direct numerical integration fails for the very low bands where the equations become too stiff for the standard integration routines.

From the form of the multipole expansion Equation (2-12) (main text) it follows that

$$\Psi_\ell(g,z') = e^{ik'z'} \sum_{L'_z} b(g,L'_z)\, e^{iL'_z z'} \qquad \text{(D-7)}$$

D-1 Martinez, G., Schluter, M., and Cohen, M. L., Phys. Rev. B, Vol. 11, No. #, 1975, p. 651.

D-2 Kohn, S. E., Yu, P. Y., Petroff, Y. R., Shen, Y. Tsang, and Cohen, M. L., Phys. Rev. B, Vol. 8, No. #, 1973, p. 1477.

where $b(g,L_z')$ are coefficients to be determined. Obviously, Equation (D-7) has the correct Bloch periodicity. Furthermore, invoking Equations (2-3), and (2-4) yields

$$L_z' = \frac{2\pi}{a^*} N \quad , \quad N = n_1 + n_2 + n_3 \tag{D-8}$$

where $a^* = a\sqrt{3}$, Equation (4-7b), and n_1, n_2, $n_3 = 0, \pm 1, \pm 2, \ldots$ from Equation (2-4). Equation (D-8) implies that for a given g the sequence of allowed N(n) values is <u>restricted</u> to the series given in Table 1-1 of main text. These values are either of the form 3m (m is an integer) or the complementary set of integers. Imposing these restrictions on N(n) is <u>essential</u> to avoid spurious degeneracy between the bands for K = 1 and K = 1/3 and to reduce the size of the secular equation. Hence, the plane wave expansion used is:

$$\Psi_\ell(g,z') = \sum_{n=-N_w}^{N_w} b_n(g) \exp\left[\frac{2\pi i}{a^*} z' \left(N(n) + \frac{3}{2} K\right)\right] \tag{D-9}$$

and N(n) is specified for each g-value in Table 1-1.

Inserting Equation (D-9) into the wave equations and projecting the individual plane waves yields a secular equation for $E_n(k)$. The matrix elements $\langle n|v_m(g_p,z')|n'\rangle$ are evaluated using a Fast Fourier Transform algorithm. The eigenvalues are obtained by searching for $E_n(\vec{k})$ which make the secular equation determinant vanish. Unphysical $E_n(\vec{k})$ can be identified by considering the coefficients $b_n(g)$. For an unphysical $E_n(\vec{k})$ these coefficients nearly vanish for one or more of the multipoles or they do not vanish for the proper N(n).

At the L-point (K = 1, Equation (3-7b), main text) every multipole has a definite z'-parity, Table 3-4. Combining this with the Bloch periodicity Equation (4-7) (main text) yields

$$\Psi_\ell(g_F,\ z' = a^*/2-\zeta) = -\pi_z\ \Psi_\ell(g_F,\ z' = a^*/2+\zeta) \tag{D-10a}$$

where

$$-a^*/2 \le \zeta \le a^*/2 \tag{D-10b}$$

Equation (D-10) implies sign-relations between the proper pairs of $b_n(g)$. In this manner we distinguish between the L_1 and L_2' bands. For $K \neq 1$, all bands belong to the Λ_1 symmetry (compare Tables 3-3 and 3-4 (main text) to obtain the compatability relations from the ℓ-parity). Note from Tables 3-3, 3-4 that including the ℓ=0 multipole is essential to differentiate between the L_1, L_2' and the L_1', L_2 representations.

Our experience indicates that taking $N_w = 7$ in Equation (D-9) is sufficient.

DISTRIBUTION

	Copies
Office of the Chief of Naval Research	
Attn: ONR-1114	
(Dr. G. Wright)	1
(Dr. D. Liebenberg)	1
800 No. Quincy Street	
Arlington, VA 22217-5000	
National Technical Information Service (NTIS)	
Springfield, VA 22161	1
Experimental Station	
DuPont de Nemours & Company	
Attn: R. V. Kasovski	1
Wilmington, DE 19898	
Library of Congress	
Attn: Gift & Exchange Division	4
Washington, DC 20540	
Defense Technical Information Center	
Cameron Station	
Alexandria, VA 22304-6145	12

Internal Distribution:		Copies
E231		2
E232		3
R41		1
R41	(D. Agassi)	3
R43	(J. Restorff)	1
R41	(T. Chu)	1
R43	(K. Hathaway)	1
R43	(J. Cullen)	1

REPORT DOCUMENTATION PAGE

Form Approved OMB No. 0704-0188

1. AGENCY USE ONLY *(Leave blank)*	2. REPORT DATE	3. REPORT TYPE AND DATES COVERED
	15 June 1991	

4. TITLE AND SUBTITLE
PSEUDOPOTENTIAL BAND CALCULATIONS ALONG A HIGH-SYMMETRY AXIS: PART I--Central Potential and the [111] Direction

5. FUNDING NUMBERS

6. AUTHOR(S)
D. Y. Agassi and J. B. Restorff

7. PERFORMING ORGANIZATION NAME(S) AND ADDRESS(ES)
Naval Surface Warfare Center
White Oak laboratory (Code R41)
10901 New Hampshire Avenue
Silver Spring, MD 20903-5000

8. PERFORMING ORGANIZATION REPORT NUMBER
NAVSWC TR 91-324

9. SPONSORING/MONITORING AGENCY NAME(S) AND ADDRESS(ES)

10. SPONSORING/MONITORING AGENCY REPORT NUMBER

11. SUPPLEMENTARY NOTES

12a. DISTRIBUTION/AVAILABILITY STATEMENT
Approved for public release; distribution is unlimited.

12b. DISTRIBUTION CODE

13. ABSTRACT *(Maximum 200 words)*

A method for band structure calculations along a high-symmetry axis is introduced in this report. It entails a cylindrical coordinate multipole expansion of the wave function and an exact reduction of the three-dimensional Schrodinger equation into a set of one-dimensional wave equations for the multipoles. Group theoretic considerations and energy arguments imply good convergence, regardless of the unit-cell extension along the high-symmetry direction. Band calculations of a test case, PbSe along the [111] direction, demonstrate the good convergence. This method is expected to be particularly useful for structures highly anisotropic along a high-symmetry axis, e.g., superlattices.

14. SUBJECT TERMS
high-symmetry axis; multipole expansion; wave equations; superlattices; band structure calculations; spin orbit interaction

15. NUMBER OF PAGES
58

16. PRICE CODE

17. SECURITY CLASSIFICATION OF REPORT	18. SECURITY CLASSIFICATION OF THIS PAGE	19. SECURITY CLASSIFICATION OF ABSTRACT	20. LIMITATION OF ABSTRACT
UNCLASSIFIED	UNCLASSIFIED	UNCLASSIFIED	UL